Kinase interplay centered on two regulatory elements confines the checkpoint protein Lte1 to the bud cell cortical compartment

Marco Geymonat[‡], Qiuran Peng[‡^*], Hanlu Chen[‡^], Sneha Parmar[‡], Helen Mott[§], Darerca Owen[§] and Marisa Segal[‡]

^ equal contributors

[‡] Department of Genetics, University of Cambridge, Downing Street, Cambridge CB2 3EH, UK
[§] Department of Biochemistry, University of Cambridge, 80 Tennis Court Rd., Cambridge CB2 1GA, UK

* Current address: Oncology R&D, The Discovery Centre-AstraZeneca, Biomedical Campus, 1 Francis Crick Ave, Cambridge CB2 0AA, UK

Correspondence should be addressed to
Marco Geymonat (mg604@cam.ac.uk) and Marisa Segal (ms433@cam.ac.uk)
Tel: +44 1223 760527 +44 1223 766744

Running header: Phospho-regulation of Lte1 cortical localization

Keywords: cell cycle, polarity, protein kinase, small GTPases, GEF, checkpoint

Abbreviations: CDK, cyclin-dependent kinase; CHD, Cdc25 homology domain; GAP, GTPase activating protein; GEF, guanine nucleotide exchange factor; LRE, Lte1 regulatory element; MEN, mitotic exit network; PAK, p21-activated kinase; REM, Ras exchanger motif; SPB, spindle pole body; SPOC, spindle position checkpoint.

ABSTRACT

In budding yeast, Lte1, a component of the spindle position checkpoint, must be confined to the bud for correctly coupling chromosomal segregation across the bud neck with mitotic exit. Bud compartmentalization involves a phospho-dependent program with Ras-GTP acting as the ultimate cortical anchor. Here we have dissected this program by identifying an Lte1 domain participating in Ras binding and two phospho-regulatory motifs, the N- and C-LREs (Lte1 Regulatory Elements). The C-LRE mediates control of Lte1 cortical recruitment by the p21-activated kinase, Cla4. The N-LRE modulates Lte1 binding to Ras more directly and is phosphorylated by the yeast MARK/PAR-1 protein kinases, Kin1/2. Along with previously described CDK phosphorylation sites, the N- and C-LREs were required for Lte1 localization and timely mitotic exit. These studies uncover the coordinated interplay between multiple protein kinases allowing Lte1 to integrate cell polarity and cell cycle cues for strict compartmentalization at the bud cell cortex.

INTRODUCTION

Spatial and temporal coordination between chromosomal segregation and the division plane is crucial to cellular integrity over cell divisions. In the particular case of an asymmetric cell division, the cell polarity and cell cycle machineries collaborate to define opposite cortical compartments with the intended division site in between. These not only support navigational cues to bias the orientation of the mitotic apparatus and thus specify the division plane, but also lay out the foundations for differential daughter cell identity and age (Casas Gimeno and Paridaen, 2022; Guo and Dong, 2022; Habib and Acebron, 2022; Pineau et al., 2023; Yamashita, 2023).

Mitotic exit control in the budding yeast *Saccharomyces cerevisiae* is a remarkable paradigm for exploring the role of cortical domain demarcation in underpinning coordination between the mitotic apparatus and the cytokinetic plane (Baro et al., 2017; Caydasi and Pereira, 2012; Geymonat and Segal, 2017). Highly polarized growth in yeast generates a daughter (bud) connected to the mother cell through the bud neck, a narrow constriction serving as the site for cell division (Chiou et al., 2017; Marquardt et al., 2021; Okada et al., 2013; Spiliotis and McMurray, 2020). Crucially, mitotic exit and cytokinesis can only occur after the mitotic spindle that elongates from the mother cell has crossed the bud neck, thus bringing a set of the duplicated chromosomes into the daughter cell. This precondition for division in budding yeast hinges on the regulated release of the phosphatase Cdc14 from sequestration in the nucleolus by two signaling pathways acting in tandem: the Fourteen Early Anaphase Release (FEAR) network promoting transient Cdc14 nuclear spread, followed by the Mitotic Exit Network (MEN) causing sustained and more complete release throughout the cell (Queralt and Uhlmann, 2008; Rock and

Amon, 2009; Shou et al., 1999; Stegmeier et al., 2002; Visintin et al., 1999). The ensuing dephosphorylation of critical cyclin-dependent kinase (CDK) substrates, sets in motion irreversible mitotic exit and cytokinesis (Jaspersen et al., 1999; Jaspersen et al., 1998; Visintin et al., 1998).

A surveillance mechanism known as the Spindle POsition Checkpoint (SPOC), restricts MEN activation until one pole of the spindle has entered the bud compartment (Bardin et al., 2000; Caydasi and Pereira, 2012; Pereira et al., 2000). According to a long-standing model, the SPOC controls the GDP-GTP switch of the small GTPase Tem1 (Scarfone and Piatti, 2015; Shirayama et al., 1994b), the upstream trigger of the MEN protein kinase cascade that promotes Cdc14 sustained release. Tem1 is localized to the Spindle Pole Body (SPB, the counterpart of the animal centrosome) together with its negative regulator Bub2-Bfa1, a two-component GTPase-activating protein (GAP) that stimulates conversion of GTP-bound Tem1 to its GDP-bound inactive state (Bardin et al., 2000; Geymonat et al., 2002; Pereira et al., 2000; Shirayama et al., 1994b). To date, a Tem1 guanine nucleotide exchange factor (GEF) has not been identified. Instead, inhibition of the GAP contributes to Tem1 activation. Two protein kinases modulate Tem1 via its GAP in an antagonistic fashion. Inhibitory phosphorylation of Bfa1 by the polo-like kinase Cdc5 results in active Tem1 (Geymonat et al., 2003; Hu et al., 2001). Conversely, Kin4 phosphorylation of Bfa1 blocks GAP downregulation by Cdc5 keeping Tem1 inactive. Importantly, Kin4 is confined to the mother cell (D'Aquino et al., 2005; Pereira and Schiebel, 2005) and opposed by Lte1, a protein restricted to the bud cortical compartment (Bardin et al., 2000; Pereira et al., 2000).

Lte1 shares sequence similarity with the catalytic module of Ras-GEFs (Boguski and McCormick, 1993; Shirayama et al., 1994a). In canonical Ras-GEFs, this module consists of two contiguous segments (Bos et al., 2007): the Ras Exchanger Motif (REM) and the Cdc25 Homology Domain (CHD), the GEF active site first identified in the yeast Ras-GEF Cdc25 (Broek et al., 1987; Camonis et al., 1986; Robinson et al., 1987). In Lte1, separate REM and CHD-like sequences map to Lte1's N and C-termini, respectively. However, the logical expectation that Lte1 could be the Tem1-GEF has not been met experimentally. Instead, REM and CHD-like sequences have been implicated in Lte1 cortical anchoring via Ras-GTP (Geymonat et al., 2009; Geymonat et al., 2010; Seshan and Amon, 2005; Yoshida et al., 2003). In turn, a central region of Lte1 binds and inhibits Kin4 (Bertazzi et al., 2011; Falk et al., 2016a; Falk et al., 2011).

Collectively, these findings laid the premise for the "two-zone model" in which the SPB supports a spatial sensor that is switched on upon entry in the bud (Bertazzi et al., 2011; Chan and Amon, 2010; Falk et al., 2011). Briefly, spindle alignment along the mother-bud axis instructs progressive Bub2-Bfa1-Tem1 polarization to the SPB committed to the bud (Caydasi and Pereira, 2009; Monje-Casas and Amon, 2009; Pereira et al., 2001). Elongation of the spindle across the bud neck satisfies the SPOC: Tem1 on the leading SPB escapes Kin4 inhibitory action as it enters the Lte1-marked bud compartment in which GAP downregulation by Cdc5 and concomitant Tem1 activation take effect (Caydasi and Pereira, 2009; Falk et al., 2016b; Fraschini et al., 2006; Monje-Casas and Amon, 2009). However, the role of Tem1 as a canonical GTPase switch has been recently brought to question (Zhou et al., 2024). This new study posits instead that the GTPase cycle would govern Tem1 recruitment to the SPB. In this scenario, it would be the rise in Tem1 effective

concentration at the leading pole that conveys the signal for activation of the MEN kinase cascade. Furthermore, Lte1 may additionally activate mitotic exit in a Kin4-independent manner by an, as yet, unknown mechanism (Caydasi et al., 2017; Falk et al., 2016a).

Cdc42, the master regulator of cell polarity (Chiou et al., 2017), is required for Lte1 cortical recruitment at the incipient bud following G1-CDK activation. Yet, it is dispensable for maintaining Lte1 bud cortex association, suggesting multiple mechanisms are at play to secure Lte1 cortical retention past bud emergence. Furthermore, an intact septin ring is essential to confine Lte1 to the bud (Hofken and Schiebel, 2002; Jensen et al., 2002; Seshan et al., 2002). Lte1 exhibits prominent cell cycle-dependent phosphorylation (Bardin et al., 2000; Lee et al., 2001) attributed to two protein kinases so far: the p21-activated kinase (PAK) Cla4 and CDK (Bardin et al., 2000; Hofken and Schiebel, 2002; Jensen et al., 2002; Seshan et al., 2002; Ubersax et al., 2003). Previous studies have correlated Lte1 phosphorylated state with cortical association and binding to Ras (Geymonat et al., 2010; Jensen et al., 2002; Seshan and Amon, 2005; Seshan et al., 2002). Phosphorylation, cortical association and binding to Ras are reversed by the phosphatase Cdc14 (Jensen et al., 2002; Seshan and Amon, 2005; Seshan et al., 2002). Ras and Cla4 may be interdependent for promoting the Lte1 phosphorylated state and establishing Lte1-Ras complexes at the cell cortex (Seshan and Amon, 2005). Accordingly, bulk phosphorylation of Lte1 is abrogated in either *cla4*Δ or *ras1*Δ *ras2*Δ mutants, along with Lte1 cortical association (Hofken and Schiebel, 2002; Seshan and Amon, 2005; Yoshida et al., 2003). Conversely, *ras1*Δ *ras2*Δ mutations prevent overexpressed Cla4 from enhancing Lte1 recruitment to polarized cortex (Seshan and Amon, 2005).

Here we have dissected phospho-dependent control of Lte1 cortical recruitment and compartmentalization with reference to Lte1-Ras complex formation. First, we defined the minimal Lte1 sequence requirements for this program. This analysis implicated the REM-like domain in cortical anchoring via Ras-GTP and pointed to the significance of two distinct phospho-site clusters as Lte1 Regulatory Elements or LREs. The C-LRE next to the CHD was a target of Cla4 *in vitro* and phospho-mimetic substitutions within this element restored Lte1 cortical localization in a *cla4*Δ background. By contrast, phospho-mimetic substitutions in the N-LRE adjacent to the REM enhanced intrinsic binding to Ras-GTP resulting in Lte1 breaching compartmentalization with localization favoring the mother cell cortex. Furthermore, we found that the yeast MARK/PAR-1 protein kinases Kin1/2 (Levin et al., 1987; Wu and Griffin, 2017; Yuan et al., 2016) contributed to N-LRE phosphorylation and ensuing enhancement of Lte1 binding to Ras-GTP i*n vitro*. Finally, cancelling phospho-sites in the N-LRE and C-LRE along with previously described CDK sites (Jensen et al., 2002) disrupted the Lte1 cortical localization program with a concomitant perturbation of mitotic exit. Taken together, our studies uncover an orderly interplay between multiple protein kinases allowing Lte1 to integrate cell polarity and cell cycle controls enforcing its strict compartmentalization at the bud cell cortex.

RESULTS

Exploring Cla4-dependent control of Lte1 localization by still-imaging analysis

In agreement with previous studies (Bardin et al., 2000; Hofken and Schiebel, 2002; Seshan et al., 2002), the mobility shift of a Lte1-Protein A (ProA) fusion due to phosphorylation *in vivo* was markedly suppressed in a *cla4*Δ mutant (Figure 1 A). Yet, according to the Saccharomyces Genome Database (SGD, https://www.yeastgenome.org/), Lte1 undergoes phosphorylation at ~80 sites, with only 2 responding to the PAK consensus R/K-R-X-pS/T and 4 to the minimal Cla4 consensus R-X-pS/T (Mok et al., 2010). Lte1 is a known CDK substrate (Jensen et al., 2002) but potentially multiple unidentified protein kinases also target Lte1.

In order to genetically dissect the phosphoregulatory mechanisms underlying the Lte1 program of localization, a quantitative framework based on live imaging analysis of asynchronous cell cultures was developed and applied, in the first instance, to unperturbed populations of otherwise wild type or *cla4*Δ cells expressing Lte1^{WT}-GFP (Figure 1 B-D). Still images of cells from asynchronous populations ordered by morphology recapitulated the program of Lte1 cortical localization in wild type cells in agreement with time lapse analysis (Supplement to Figure 1 A). Briefly, Lte1^{WT}-GFP underwent recruitment at bud emergence (Figure 1 B, a) and extended over the entire bud surface during bud growth (Figure 1 B, b-d). Following mitotic exit, delocalized label became diffuse but transiently marked the division site (Figure 1 B, e). Finally, Lte1-GFP in the former mother cell underwent recruitment to the new incipient bud while continuing to form a broad crescent near the former division site in the daughter cell (Figure 1 B, f) until a new budding site was selected. By contrast,

Lte1^{WT}-GFP was only weakly recruited to the incipient bud over cytoplasmic label background in *cla4*Δ cells (Figure 1 B, g) and remained essentially apical during bud growth (Figure 1 B, h-j), returning to the division site at mitotic exit (Figure 1 B, k) until recruitment at the new incipient bud (Figure 1 B, l). The mutation did not affect Lte1^{WT}-GFP expression level (Supplement to Figure 1 B). Weak apical localization was the predominant label distribution collectively scored in *cla4*Δ budded cells (Figure 1 C and Supplement to Figure 1 C).

Single-cell linescan analysis along the mother-bud axis was implemented to obtain a one-dimensional quantitative description of Lte1 distribution in terms of cortical spread (the width of the linescan peak at half maximal value) or mean intensity as a function of bud cell length (Figure 1 D). Consistent with the qualitative assessment in Figure 1 C, Lte1 spread correlated with bud length throughout in wild type cells, while mean intensity peaked in small-budded cells and progressively declined with bud growth by dilution. This behavior essentially recapitulated a similar decline apparent by measuring mean Lte1-GFP cortical intensity in the entire bud by time lapse analysis (Supplement to Figure 1 A). For validation, average linescan traces at 0.5 µm-bud length intervals were derived from the original dataset (Supplement to Figure 1 E). In contrast to wild type cells, spread of Lte1^{WT} in *cla4*Δ cells mostly failed to scale with bud growth while initial mean intensity at the bud cell cortex was markedly decreased and further declined with bud growth. Average linescan traces from the *cla4*Δ dataset (Supplement to Figure 1 E) reflected both weak apical localization and increased cytoplasmic background label.

Taken together, a *cla4*Δ mutation virtually eliminated Lte1 phosphorylation and markedly reduced Lte1 cortical association down to limited apical label throughout

bud growth. This subtle localization retained by the *cla4*Δ strain has not been previously reported.

Lte1 sequences required for its phospho-dependent cortical association

Studies on the human Ras-GEF Son of Sevenless 1 (hSOS1) have assigned distinct roles to the REM and CHD in the GEF catalytic module: binding of Ras-GTP to the REM allosteric site enhances GDP-GTP exchange by the CHD (Margarit et al., 2003; Sondermann et al., 2004). In Lte1, sequences related to the REM and CHD map to Lte1's N- and C-termini, respectively. Those sequences are required for efficient Lte1 cortical association (Jensen et al., 2002; Yoshida et al., 2003).

In order to narrow down Lte1 target sites critical for phospho-dependent control, in-frame internal deletions were generated, preserving the REM and CHD sequences (Figure 2 A). An Lte1 construct lacking amino acids 250 to 950 exhibited cortical localization that still depended on Cla4 (Figure 2 B and C). Deletions eliminating further sequences closer to either the REM or CHD prevented cortical association (Figure 2 A). Thus, Lte1$^{\Delta 250\text{-}950}$ represented a minimal construct retaining Cla4-dependent cortical localization.

Unlike canonical Ras-GEFs, Lte1 binds solely to Ras-GTP *in vitro* and *in vivo* to direct cortical localization (Seshan and Amon, 2005; Yoshida et al., 2003). Furthermore, human H-Ras can replace yeast Ras proteins as the Lte1 cortical anchor (Supplement to Figure 2). These observations support the idea of functional conservation, perhaps pointing to a more direct involvement of the REM. To explore this possibility, the REM and CHD domains of Lte1 were modelled with two Ras

molecules bound, using the structure of the hSOS1 complex (PDB 1nvv) as a template (Figure 2 D). Based on this model, substitutions V^{102} to E and R^{103} to A were deemed analogous to those designed to prevent Ras-GTP binding to the hSOS1 REM (L^{687} to E and R^{688} to A; Sondermann et al., 2004) and were engineered into Lte1. The resulting mutant allele was referred to as *lte1*^{mREM}.

When expressed in otherwise wild type cells, Lte1^{mREM}-GFP was poorly recruited to the incipient bud and very faintly labelled the apical cortex of midsize buds (Figure 2 E and F). The observed label was too weak for digital quantification. It was notable that this distribution mode was very similar to that seen when Lte1^{WT}-GFP was expressed in cells in which both yeast *RAS* genes were disrupted, supporting the idea that substitutions within the REM disabled anchorage via Ras (Supplement to Figure 2). Furthermore, western blot analysis indicated a marked decrease in bulk phosphorylation of Lte1^{mREM}-ProA *in vivo*, with a subtle mobility shift dependent on Cla4 still detected (Figure 2 G). Finally, substitutions within the REM also compromised Lte1's ability to rescue the synthetic lethality between *lte1*Δ and the FEAR mutation *spo12*Δ (Figure 2 H).

In conclusion, these data demonstrate that sequences adjacent to the REM and CHD were required for Cla4-dependent Lte1 localization and may therefore contain phospho-regulatory sites. In addition, the Lte1 REM might act as a Ras-GTP binding site analogous to that in hSOS1 and be key to Ras-GTP mediated cortical association.

Phospho-mimetic substitutions at a site adjacent to the REM directed Lte1 to the mother cell cortex, independent of Cla4

Previous phospho-proteomic studies (Holt et al., 2009; Lanz et al., 2021) identified a 6 phospho-site cluster proximal to the REM within sequences present in $Lte^{\Delta 250-950}$ (Figure 3 A). In order to address its significance, we reasoned that gain-of-function phospho-mimetic substitutions would be particularly revealing, given the correlation between Lte1 phosphorylated state and cortical association. In view of the results presented here, we now refer to this phospho-regulatory motif as N-Lte1 Regulatory Element or N-LRE.

Otherwise wild type strains expressing the mutant versions $Lte1^{N-2D}$, $Lte1^{N-4D}$ or $Lte1^{N-6D}$ (Figure 3 A) fused to GFP exhibited significant cortical association with the mother cell, demonstrating that they breached compartmentalization. Furthermore, $Lte1^{N-4D}$ and $Lte1^{N-6D}$ displayed particular bias to the mother cell cortex (Figure 3 B and Supplement to Figure 3 A).

Further characterization was pursued using $Lte1^{N-4D}$ (Figure 3 C-E). Cortical association of $Lte1^{N-4D}$-GFP was already apparent in 92 % of unbudded cells (Figure 3 C, a) and continued to favor mother cells after bud emergence (Figure 3 C, b-c and Figure 3 D). $Lte1^{N-4D}$ cortical association was independent of Cla4 (Figure 3 C, d and Figure 3 D). Yet, overall cortical localization was markedly lost with the addition of REM substitutions presumed to disrupt binding to Ras-GTP ($Lte1^{N-4D-mREM}$, Figure 3 C, e-f and Figure 3 D), demonstrating that the phospho-mimetic residues could bypass phospho-regulation but not the requirement for an intact REM.

Previous studies have repeatedly pointed to the close relationship between Lte1 cortical association, phosphorylation and complex formation with Ras-GTP (Bardin et al., 2000; Geymonat et al., 2010; Seshan and Amon, 2005; Seshan et al., 2002). It was therefore crucial to determine the impact of phospho-mimetic substitutions within the N-LRE on those processes.

First, a series of strains expressing Lte1^{WT} or Lte1$^{N\text{-}4D}$ fused to ProA in a wild type or *cla4*Δ background was constructed to assess bulk phosphorylation of Lte1 *in vivo* in cells synchronized at metaphase (Figure 3 E). In contrast to Lte1^{WT}, Lte1$^{N\text{-}4D}$ retained a considerable mobility shift in a *cla4*Δ background. This was also the case for Lte1$^{N\text{-}2D}$ and Lte1$^{N\text{-}6D}$ (Supplement to Figure 3 B). Yet, the mobility shift was essentially lost if the REM substitutions that prevented cortical association were additionally present (Figure 3 E). These data suggest that constitutive, Cla4-independent cortical association restored Lte1 phosphorylation by other protein kinases outside the N-LRE.

Second, Lte1 binding to Ras-GTP *in vitro* was assessed by pull-down assays using purified Lte1^{WT} or mutant versions fused to MBP as bait (Figure 3 F and G). Relative to Lte1^{WT}, substitutions within the REM (Lte1^{mREM}) or an in-frame deletion encoding solely joint REM-CHD sequences (Lte1$^{\Delta 165\text{-}1144}$) markedly reduced binding to Ras-GTP. The N-terminal 950 amino acids retained very limited binding (Figure 3 F), pointing to an important contribution by C-terminal sequences consistent with the deletion analysis *in vivo* (Figure 2 A). Phospho-mimetic substitutions within the N-LRE in full length Lte1 (Figure 3 F) or in the context of Lte1$^{\Delta 250\text{-}950}$ (Figure 3 G) appeared to enhance binding to Ras-GTP, an effect abrogated by additional substitutions within the REM (Lte1$^{N\text{-}4D\text{-}mREM}$, Figure 3 F). Yet, those phospho-mimetic

substitutions in the context of the N-terminal 950 amino acid fragment failed to enhance binding to Ras-GTP, underscoring a requirement for a C-terminal domain. Pull-down assays followed by quantitative western blot analysis were performed to compare the binding abilities of the different phospho-mimetic substitution mutants within the N-LRE (Supplement to Figure 3 C-D). For all mutants, binding to Ras-GTP was markedly increased.

Taken together, these experiments indicated that phospho-mimetic substitutions within the N-LRE enhanced binding to Ras-GTP leading to deregulated complex formation *in vivo* which translated into constitutive cortical association superseding cell cycle-dependent phosphoregulatory control.

The key premise of the SPOC is that mutually exclusive inhibitory and permissive compartments to mitotic exit are set by Kin4 in the mother cell and Lte1 in the bud, respectively. Mutants impaired for spindle positioning across the bud neck, e.g., *dyn1*Δ (a deletion of the dynein heavy chain gene) accumulate budded cells containing elongated spindles within the mother cell as a result of a SPOC-enforced delay, a phenotype enhanced by incubating cultures at 14°C (Li et al., 1993). Mitotic exit can only occur after the spindle repositions across the bud neck, thus satisfying the checkpoint. Ectopic localization of Lte1 to the mother compartment will lift this restriction (Bertazzi et al., 2011). The impact of phospho-mimetic substitutions at the N-LRE on checkpoint performance was therefore determined in *dyn1*Δ mutant cultures by scoring collectively re-budding and re-duplication of spindle poles marked by Spc29-CFP to determine the proportion of cells undergoing inappropriate mitotic exit and progression into the subsequent cell cycle (Figure 3 H and Supplement to Figure 3 E).

As expected, the *LTE1*^{WT} *dyn1*Δ culture was markedly enriched for large-budded cells with mispositioned anaphase spindles, indicative of a SPOC-imposed delay. The additional introduction of *bfa1*Δ, a mutation that disables the SPOC, depleted this category and increased instead cells undergoing re-budding and SPB re-duplication due to inappropriate mitotic exit. Similarly, *LTE1*$^{N\text{-}4D}$ *dyn1*Δ and, to a lesser extent *LTE1*$^{N\text{-}2D}$ *dyn1*Δ strains pre-empted mitotic exit, as reflected by a marked accumulation of cells undergoing re-budding and re-duplication of spindle poles (Figure 3 H). It follows that phospho-mimetic substitutions within the N-LRE proved sufficient not only to breach Lte1 compartmentalization but also to disrupt checkpoint function, highlighting the importance of correct phospho-dependent cell cycle-regulated formation of a complex between Lte1 and Ras-GTP to secure its bud confinement.

The functional importance of cancelling N-LRE mediated phosphorylation was also assessed in the simplified context of Lte1$^{\Delta 250\text{-}950}$. Contrary to full-length *LTE1*, single copy *lte1*$^{\Delta 250\text{-}950}$ was unable to suppress *lte1*Δ *spo12*Δ synthetic lethality but displayed manifest suppression when carried in a multicopy plasmid (Figure 3 I). In the same context, substitutions at the REM, even when combined with the phospho-mimetic N-4D prevented rescue. Finally, substitutions that cancelled phosphorylation at the N-LRE (N-6A) prevented suppression, pointing to the requirement of phosphorylation at the N-LRE for Lte1$^{\Delta 250\text{-}950}$ function *in vivo.*

C-LRE, a second phosphoregulatory site adjacent to the CHD

Lte1 is a substrate of Cla4 and CDK, yet no connection has been made between the functional impact of particular phosphorylation sites and either protein kinase. In

order to address this question, Cla4 and CDK *in vitro* kinase assays were performed with purified Lte1 truncations as substrates, designed to focus on the N-LRE (as it contains at least one potential phosphorylation site for each kinase). Analogue-sensitive CDK-as complexes (Bishop et al., 2000), Cla4 and Cla4^{KD} (kinase-dead) were also purified from yeast (Figure 4 A-C). The N-terminal truncation Lte1$^{1-325}$ was a specific substrate for both CDK and Cla4 (Figure 4 B), as phosphorylation did not occur in the presence of the inhibitory analog 1NM-PP1 or with a kinase-dead version of Cla4, respectively. However, phosphorylation persisted when the N-LRE sites were cancelled by S to A substitutions (N-2A, N-4A or N-6A). An in-frame deletion consisting of the REM and CHD (Lte1$^{\Delta 165-1144}$) showed markedly reduced phosphorylation with either kinase. When a similar kinase assay was implemented using Lte1$^{\Delta 250-950}$ as substrate, radioactive incorporation increased but substitutions within the N-LRE failed to reveal specific phosphorylation at that sequence by CDK or Cla4. Importantly, a deletion that eliminated the sequence proximal to the CHD only (Lte1$^{\Delta 250-1144}$) markedly reduced phosphorylation *in vitro* by either kinase (Figure 4 C). This pointed to a second set of phospho-sites between amino acids 950-1144, as suggested by phospho-proteomic studies curated by the SGD. Lte1 versions containing substitutions to cancel this second set of phospho-sites were generated and used as substrates for kinase assays *in vitro* (Figure 4 D).

In the context of Lte1$^{\Delta 250-950}$, S to A substitutions at S^{956}, S^{969}, S^{979}, S^{1105}, S^{1109}, and S^{1116} (C-6A) reduced phosphorylation by either CDK or Cla4 *in vitro* (Figure 4 E and F) without further decrease when combining those with substitutions within the N-LRE (12A). Phosphorylation by Cla4 was similarly reduced when substitutions were introduced at S^{1105}, S^{1109}, and S^{1116} only (C-3A) but phosphorylation by CDK continued (Figure 4 G). Taken together, the sub-cluster closest to the CHD, referred

to here as C-LRE was a prime target of Cla4 and contained one full PAK consensus site (R/K-R-X-pS/T). Further CDK sites were identified near this element.

Phospho-mimetic substitutions at the C-LRE restored Lte1 recruitment to the bud cell cortex in a *cla4*Δ mutant

In order to determine the role of phosphorylation at the C-LRE we first expressed a mutant containing 6 phospho-mimetic substitutions ($Lte1^{C\text{-}6D}$; Figure 4 D) fused to GFP in otherwise wild type cells. The protein was correctly confined to the bud cortex compartment (Supplement to Figure 5 A). Yet, the significance of part of these phospho-sites became apparent when $Lte1^{C\text{-}6D}$-GFP and $Lte1^{C\text{-}3D}$-GFP (Figure 4 D) were expressed in a *cla4*Δ background (Figure 5 A-C). By contrast to the impaired cortical recruitment observed for $Lte1^{WT}$-GFP in *cla4*Δ cells, $Lte1^{C\text{-}6D}$-GFP and $Lte1^{C\text{-}3D}$-GFP decorated the entire bud cortex with limited cytoplasmic background, the prevalent mode of localization in budded cells (Figure 5 A and B).

Single-cell linescan analysis was implemented to quantify spread and mean cortical label intensity in the bud over a population as a function of bud size (Figure 5 C). By contrast to the limited spread and recruitment observed for wild type Lte1 in a *cla4*Δ background, $Lte1^{C\text{-}6D}$ and $Lte1^{C\text{-}3D}$ retained localization to a comparable degree while bud cortical spreading scaled with bud growth, in agreement with the qualitative assessment. However, maximal mean intensity in small budded cells was below that observed for $Lte1^{WT}$ in wild type cells (compare with Figure 1 D). Average linescan traces from the same dataset confirmed this observation. For both $Lte1^{C\text{-}6D}$ and $Lte1^{C\text{-}3D}$, initial peaks corresponding to small budded cells were reduced relative to

Lte1^{WT} in wild type cells (compare Supplement to Figure 5 C with Supplement to Figure 1 E). The incomplete rescue could be due to the contribution by additional Cla4 sites outside the C-LRE. Yet, this result is also consistent with previous proposals that Cla4 might help tethering Lte1 to the cell cortex by physical interaction as well as through alternative Cla4-dependent anchors (Seshan et al., 2002).

Lte1$^{C\text{-}6D}$ and Lte1$^{C\text{-}3D}$ were hyper-phosphorylated *in vivo* contrary to Lte1^{WT} when expressed in a *cla4*Δ background, as indicated by manifest mobility-shift observed by western blot analysis (Figure 5 D). Yet, Cla4-dependent phosphorylation was still detected (compare the upper low mobility bands in *CLA4* vs *cla4*Δ lanes for each Lte1 variant) either due to additional Cla4 sites away from the C-LRE or another indirect contribution by Cla4. These data collectively support the idea that other protein kinases may phosphorylate Lte1 once recruited to the cell cortex and/or dependent upon priming phosphorylation by Cla4. However, phospho-mimetic substitutions within the C-LRE bypassed dependency on Cla4 without otherwise disrupting compartmentalization of Lte1 to the bud.

A MARK/PAR-1-like kinase targets N-LRE sites

The fact that phospho-mimetic substitutions within the C-LRE restored a phospho-dependent mobility shift linked to restricted bud cortex association in a *cla4*Δ background (i.e. without breaching compartmentalization) suggested the participation of additional bud-localized protein kinases that could target the N-LRE among other sites.

Yeast Kin1 and Kin2 are members of the MARK/PAR-1 conserved family of S/T protein kinases (Wu and Griffin, 2017). Kin1 and Kin2 have been implicated in control of cell polarity, polarized trafficking and the ER stress response (Anshu et al., 2015; Elbert et al., 2005; Ghosh et al., 2021). Kin2 is enriched at sites of polarized growth and can interact with the polarisome component Pea2, the septin Cdc11 and Rho3 (Yuan et al., 2016). Kin1 and Kin2 are functional homologues that share extensive sequence identity (Levin et al., 1987) and the consensus motif N-X-pS-X-S/T-X-I/L, which includes a potential phospho-priming site at position +2 targeted by an unknown kinase, as proposed by Jeschke et al. (2018). The N-LRE contains a close match to this consensus, pointing to the possibility that yeast Kin1 and Kin2 protein kinases might regulate Lte1 (Figure 6 A).

Thus, localization studies were conducted after introducing phospho-mimetic substitutions solely at the putative Kin1/2 site in the N-LRE. The resulting Lte1$^{219D, 222D}$-GFP fusion expressed in otherwise wild type cells was localized to the cortex of unbudded cells as well as the mother cell cortex of budded cells. Modes of cortical localization were comparable to those observed for Lte1$^{N\text{-}4D}$ but the bias to the mother cell cortex was less pronounced (Figure 6 B).

Supporting the idea of direct control, purified Kin2 phosphorylated Lte1$^{\Delta 250\text{-}950}$ *in vitro* (Figure 6 C) while no incorporation was observed with Kin2^{KD} (kinase-dead). Furthermore, the phosphorylated band was markedly reduced when substitutions cancelling phosphorylation sites in the N-LRE were introduced (Figure 6 C, N-6A or 12A) but was retained when such substitutions were introduced at the C-LRE only (Figure 6 C, C-6A). Taken together, Kin2 phosphorylates Lte1 at the N-LRE.

Then, the contribution of Kin1/2 to bulk Lte1 phosphorylation *in vivo* was assessed by western blot analysis of whole cell extracts from strains expressing Lte1^{WT}-ProA or Lte1$^{C\text{-}6A}$-ProA in wild type or *kin1*Δ *kin2*Δ background (Figure 6 D). A subtle decrease in mobility shift was observed for Lte1^{WT}-ProA expressed in *kin1*Δ *kin2*Δ relative to wild type backgrounds. Lte1$^{C\text{-}6A}$-ProA also exhibited a reduced mobility shift compared to Lte1^{WT}-ProA which was further reduced when expressed in *kin1*Δ *kin2*Δ cells. Thus, Kin1/2-dependent phosphorylation and substitutions at the C-LRE showed a cumulative effect on bulk phosphorylation *in vivo*, consistent with the idea that Kin1/2 phosphorylates Lte1 but does not target the C-LRE (Figure 6 D). Conversely, Lte1$^{219D,\ 222D}$-ProA retained an *in vivo* phospho-dependent mobility shift in a *cla4*Δ background, in line with the connection between restored cortical association and phosphorylated state contributed by alternative protein kinases (Supplement to Figure 6 A).

Live imaging suggested that Lte1^{WT}-GFP localization was mildly impaired in *kin1*Δ *kin2*Δ cells (Figure 6 E and F). Single-cell linescan analysis was therefore implemented to characterize any dependency on Kin1/2 for Lte1 localization in a cell population (Figure 6 G). While the spread of the label continued to scale with bud growth, an overall reduction in mean label intensity at the bud cell cortex was observed. Average linescan traces from the same dataset also reflected this overall decrease, pointing to a significant, yet redundant, contribution by Kin1/2 to the Lte1 localization program (Supplement to Figure 6 C).

In view of the observation that purified Kin2 could phosphorylate sites within the Lte1 N-LRE and that phospho-mimetic substitutions directed Lte1 to the mother cell cortex, it was of great interest to explore the direct impact of Kin2 phosphorylation on

Lte1 binding to Ras-GTP. To this end, purified MPB-Lte1 was treated with Kin2 or Kin2^{KD}, as a control prior to the pull-down assay. Only phosphorylation of the bait by active kinase increased the amount of Ras-GTP recovered by pull-down (Figure 6 H). Furthermore, MBP-Lte1$^{N\text{-}6A}$ treated in the same way showed no increase in Ras-GTP signal (irrespective of additional phospho-sites present in full-length Lte1), suggesting that Kin2-dependent enhancement was mediated by phosphorylation at the N-LRE.

In conclusion, these data identified Kin1/2 as new protein kinases contributing to the regulation of Lte1 binding to Ras-GTP as part of a phospho-dependent program for cortical localization.

Substitutions that cancel phosphorylation sites in Lte1 have a cumulative impact on Lte1 localization and function

Our analysis of substitutions that prevented phosphorylation within the Lte1 regulatory elements identified in this study, appeared to have modest effects on cell cycle-dependent localization or ability to rescue known *lte1*Δ phenotypes, in the context of full-length Lte1. By contrast, the impact of phospho-mimetic substitutions indicated that different phospho-regulatory elements support distinct mechanisms driving the program for Lte1 cortical localization. In an attempt to reconcile these observations, 12 substitutions that eliminated phosphorylation at the N-LRE, C-LRE and adjacent CDK target sites were combined (Figure 4 D). However, localization of Lte1^{12A}-GFP in otherwise wild type cells was only mildly impaired relative to Lte1^{WT}-GFP (Figure 7 A and B).

Cdc14 reverses Lte1 binding to Ras and cortical association (Jensen et al., 2002; Seshan et al., 2002), implicating CDK in Lte1 phospho-regulation. However, S/T to A substitutions at all full-consensus CDK sites within Lte1's central domain, which significantly reduced the cell cycle-dependent profile of Lte1 phosphorylation, failed to impair Lte1 localization (Jensen et al., 2002). In view of those precedents, a further mutant was generated combining the 12 A substitutions described above with those previously introduced at CDK sites in the central domain (S/T to A substitutions at positions T^{317}, T^{614}, S^{630}, S^{667}, T^{793} and S^{854}). The resulting construct, $Lte1^{18A}$-GFP, was initially localized at the incipient bud like $Lte1^{WT}$ or $Lte1^{12A}$. However, cortical label only persisted at the apical portion of the growing bud (Figure 7 A and B).

Single-cell linescan analysis confirmed the deviation from the $Lte1^{WT}$ program in a cell population expressing $Lte1^{18A}$-GFP (Figure 7 C and Supplement to Figure 7 A and B). Initial recruitment to the incipient bud site was only modestly affected and label appeared to spread over the cortex of small budded cells. Yet, label intensity further declined with bud growth, as the spread narrowed. Overall, this indicated that the bud cortical domain was not sufficiently established (yet, it is noteworthy that *lte1*^{18A} did not fully recapitulate the *cla4*Δ phenotype). Taken together, these observations point to multi-site phosphorylation over the budded interval of the cell cycle, possibly interlaced with protein-protein interactions, governing Lte1 recruitment and bud cortex retention to configure a bud cortical domain that should persist until the end of the cell cycle.

The fact that $Lte1^{18A}$ tended to localize apically in large budded cells suggested the possibility that the boundary between inhibitory and permissive domains framing the

SPOC in late mitosis might be shifted past the bud neck. If so, this might cause a mitotic exit delay despite spindle pole entry into the bud, given the presumed reduction of the permissive cortical domain marked by Lte1. To investigate this possibility, mitotic spindle progression was analyzed in *LTE1*^{WT} or *lte1*^{18A} cells expressing GFP-Tub1 (tagging α-tubulin).

Still-imaging analysis of live cells from asynchronous cultures was performed to determine the distribution of budded cells according to mitotic spindle stages (Figure 7 D). Relative to *LTE1*^{WT}, *lte1*^{18A} showed accumulation of cells containing elongated spindles, indicative of a lengthening of the anaphase interval. For further validation, time lapse analysis was performed in the same strains to directly determine the duration of spindle elongation (Figure 7 E). In agreement with the findings by still-imaging, anaphase duration was increased by 25 % in *lte1*^{18A} cells, confirming a reduced ability of Lte1^{18A} to promote timely mitotic exit. Irrespective of a delay in spindle disassembly, the *lte1*^{18A} mutation did not affect temporal coupling between spindle disassembly and cytokinesis, as previously observed in *lte1*Δ cells (Jensen et al., 2004). Still, *lte1*^{18A} retained the ability to rescue *lte1*Δ *spo12*Δ co-lethality confirming that this allele did not encode a complete loss-of-function product (Supplement to Figure 7 C).

Taken together, cumulative effects from substitutions that prevented phosphorylation of Lte1 translated into significant disruption of the program that differentially marks the bud compartment. The fact that *lte1*^{18A} continued to rescue phenotypes associated with *lte1*Δ (e.g., co-lethality with *spo12*Δ) emphasizes the significance of correctly patterning Lte1 cortical association in the bud for promoting timely mitotic exit in the unperturbed cell cycle.

Differential effect of phospho-mimetic substitutions at N-LRE vs C-LRE on Lte1-Ras2 complex formation *in vivo*

To complement the analysis for the impact of substitutions within regulatory sites on the interaction between Lte1 and Ras-GTP, the ability of Lte1 to pull down Ras-GTP *in vitro* was determined using MBP-Lte1^{WT} vs MBP-Lte1^{18A}, MBP-Lte1$^{N\text{-}6A}$ or MBP-Lte1$^{C\text{-}6D}$ as baits (Figure 8 A). We found that the inherent ability of Lte1 to bind Ras-GTP *in vitro* remained intact. Furthermore, MBP-Lte1$^{C\text{-}6D}$ did not exhibit enhanced affinity for Ras-GTP, contrasting with the effect of phospho-mimetic substitutions within the N-LRE (Figure 3).

Following these findings, we pursued the validation of the role of phospho-regulatory sites in formation of an Lte1-Ras complex *in vivo* assessed by immunoprecipitation using whole extracts from cells expressing epitope-tagged fusions of wild type or mutant Lte1 and yeast Ras2 at endogenous levels (Figure 8 B).

Ras2 was co-immunoprecipitated with Lte1^{WT}-ProA or Lte1^{18A}-ProA but was not recovered upon immunoprecipitation of Lte1^{mREM}-ProA. These observations confirmed the critical role of the REM in supporting cortical localization dependent on Ras2 binding *in vivo.* Yet, significant impairment in Ras2 co-immunoprecipitation with Lte1^{18A} was not observed. Whether this is due to poor signal dynamic range to discriminate a reduction from wild type binding level in this assay is unclear. Nevertheless, supporting the idea that constitutive cortical localization due to phospho-mimetic substitutions in the N-LRE may stem from enhanced binding to Ras, Lte1$^{N\text{-}4D}$-ProA yielded markedly increased co-immunoprecipitated Ras2, dependent on an intact REM (compare WT, N-4D and mREM N-4D-mREM).

A *cla4*Δ background prevented Ras2 co-immunoprecipitation with Lte1^{WT}-ProA, in agreement with previous studies (Seshan and Amon, 2005). Interestingly, co-immunoprecipitation was restored differently in response to phospho-mimetic substitutions at the N-LRE vs the C-LRE. Indeed, Lte1$^{N\text{-}4D}$-ProA co-immunoprecipitated Ras2 as efficiently as it did in a *CLA4* background (irrespective of the partial loss in bulk phosphorylation *in vivo* caused by the *cla4*Δ mutation, Figure 3 E). By contrast, Ras2 co-immunoprecipitation with Lte1$^{C\text{-}6D}$-ProA approximately matched the level observed for Lte1^{WT} in *CLA4* background. These data indicate that Lte1$^{N\text{-}4D}$-Ras2 complex formation may be refractive to Cla4 loss *in vivo*, and thus constitutive, due to sufficiently increased inherent affinity of Lte1 toward Ras-GTP from the outset (Figure 3 F and Supplement to Figure 3 C-D). By contrast, Lte1$^{C\text{-}6D}$-ProA mimicked a Cla4 phosphorylation event that might secure cortical tethering subject to further control confined to the bud compartment for establishment of an Lte1-Ras complex *in vivo* without otherwise affecting the inherent affinity of Lte1 towards Ras2.

These results demonstrated distinct mechanistic contributions for C vs N phospho-regulatory elements in initiating and establishing Lte1-Ras complexes, a critical sequence for enforcing exclusive Lte1 association with the bud cortical compartment.

DISCUSSION

Is the REM functionally conserved between Lte1 and hSOS1?

Lte1 cortical association via Ras requires N and C-terminal domains related to the REM and CHD of Ras-GEFs (Boguski and McCormick, 1993; Bos et al., 2007; Jensen et al., 2002; Seshan and Amon, 2005; Yoshida et al., 2003). Yet, only Ras-GTP can serve as a cortical anchor (Seshan and Amon, 2005; Yoshida et al., 2003). This selectivity might implicate the Lte1 REM as a binding site for Ras-GTP, by extrapolation from structural studies on the role of this motif in hSOS1 (Margarit et al., 2003). To establish such functional conservation, we characterized Lte1^{mREM}, a mutant encoding substitutions analogous to those shown to disrupt Ras-GTP binding to the hSOS1 REM (Sondermann et al., 2004).

In support of the conserved function of the REM, Lte1^{mREM} failed to interact with Ras *in vitro* and *in vivo* (Figure 3 F and Figure 8 B). Accordingly, Lte1^{mREM} cortical localization was severely impaired with concomitant loss of phosphorylation and function *in vivo*, although a contribution to phosphorylation by Cla4 was still detected (Figure 2 E-G). Thus, the Lte1 REM represents a critical determinant for cortical anchoring via Ras-GTP. This finding is consistent with previous deletion analysis showing that an Lte1 truncation lacking the CHD retained localization at the bud cell cortex under overexpression (Jensen et al., 2002), although a similar truncation failed to coimmunoprecipitate Ras2 from cell extracts (Yoshida et al., 2003), emphasizing that an intact CHD also contributes to efficient Ras binding *in vivo*. Indeed, substitutions at conserved residues within the CHD primary sequence prevented both cortical localization and rescue of *lte1*Δ mutant cold sensitivity

(Geymonat et al., 2009). Similarly, expression of an Lte1 truncation lacking the CHD could not rescue the synthetic lethality of *spo12*Δ *lte1*Δ cells (Seshan and Amon, 2005).

The fact that the REM and CHD map to opposite ends of Lte1 and that the protein displays self-association through N- and C-terminal sequences (Jensen et al., 2002), could prove mechanistically relevant to phospho-dependent anchoring of Lte1 to the cell cortex via Ras-GTP perhaps extending similarities between Lte1 and SOS. Indeed, activation of hSOS1 may entail both recruitment to the membrane upon signaling (through phospho-dependent docking onto an activated receptor via adaptor proteins) and conformational changes prompted by membrane association, which may lift a block to the allosteric site allowing Ras-GTP binding. This interaction would further tether hSOS1 to the cytoplasmic membrane while stimulating guanine nucleotide exchange via the CHD (Bandaru et al., 2019). In Lte1, these steps could be additionally controlled by its own phospho-regulatory elements. Furthermore, the conserved role of the REM between Lte1 and hSOS1 suggested by our findings, adds support to a previous proposal by Seshan and Amon (2005) that binding of Ras-GTP to the REM might link Lte1 cortical localization with allosteric activation of Lte1-promoted GDP-GTP exchange on Tem1. Allosteric activation might explain the failure to detect Lte1-GEF activity towards Tem1 from purified components (Geymonat et al., 2009). Collectively, these appealing ideas remain to be explored.

Polarized recruitment and anchoring via Ras are controlled by distinct Lte1 phospho-sites

Phosphorylation by Cla4 has been primarily implicated in Lte1 cortical association via Ras (Hofken and Schiebel, 2002; Seshan and Amon, 2005). In contrast to previous studies, we observed residual polarized localization of Lte1 in *cla4*Δ cells (Figure 1) and even in a *ras1*Δ *ras2*Δ mutant (Supplement to Figure 2), suggesting other intervening steps from membrane recruitment to Lte1 cortical anchoring via Ras.

In addition, the requirement for CDK activity in the program might change according to cell cycle or developmental context. In cycling cells, G1-CDK is an essential trigger for Lte1 cortical recruitment together with Cdc42 (Jensen et al., 2002). Overexpression of the CDK inhibitor Sic1 prevents Lte1-Ras coimmunoprecipitation despite polarized cortical localization and intermediate levels of Lte1 phosphorylation. Detection of Lte1-Ras immunocomplexes follows mitotic CDK activation (Geymonat et al., 2010; Seshan and Amon, 2005). Similarly, Lte1 concentrates at sites of polarized growth independent of CDK in cells arrested by mating pheromone (Jensen et al., 2002), a condition in which Lte1 does not coimmunoprecipitate Ras (Geymonat et al., 2010). The significance of this alternative program in mating cells is unknown.

To gain further mechanistic insight into phospho-dependent regulation and its links to Lte1-Ras complex formation, we first identified Lte1$^{\Delta 250\text{-}950}$, a minimal in-frame internal deletion construct that retained compartmentalized cortical localization and dependence on Cla4 (Figure 2 A-C). In this construct, two sequences we now refer

to as N-LRE and C-LRE, contained a number of potential phosphoregulatory sites that became the focus of our study. On the premise that their phosphorylation would be linked to Lte1 cortical association, we initially probed this small subset of phospho-sites for their functional significance by introducing the corresponding phospho-mimetic substitutions in the context of full-length Lte1. We then pursued *in vitro* kinase assays in an attempt to assign those key sites as targets for Cla4 or CDK. This analysis revealed contrasting roles for those two regulatory elements and led to the identification of an additional protein kinase participating in the Lte1 cortical program.

The C-LRE was a direct target for Cla4 phosphorylation (Figure 4). Phospho-mimetic substitutions within this element restored correct Lte1 localization at the bud cell cortex, phospho-dependent mobility shift and Lte1-Ras2 coimmunoprecipitation in a *cla4*Δ mutant background. Importantly, phospho-mimetic substitutions at the C-LRE and three adjacent CDK sites ($Lte1^{C\text{-}6D}$) did not enhance Lte1 binding to Ras *in vitro* or coimmunoprecipitation from cell extracts above that observed for $Lte1^{WT}$ expressed in wild type cells, consistent with the observation that the phospho-mimetic mutant remained responsive to polarizing cues and was restricted to the bud (Figures 5 and 8). Taken together, these data support a role for the C-LRE in the initial phospho-dependent recruitment of Lte1, a prerequisite for further phosphorylation directing the establishment of Lte1-Ras complexes over the bud cortex to be maintained until mitotic exit.

Phospho-mimetic substitutions within the N-LRE enhanced Lte1 binding to Ras *in vitro* and *in vivo*, thus eliminating any temporal and spatial constraints for Lte1 cortical association via Ras in cells, irrespective of Cla4 activity (Figures 3 F and 8

B). The ensuing failure to compartmentalize these Lte1 mutants compromised the SPOC (Figure 3 H). Interestingly, the extent of bias toward the mother cell cortex and SPOC defect showed a correlation with the relative strength of mutant Lte1 binding to Ras assessed by *in vitro* pull-down assays. These data indicated that the N-LRE, juxtaposed to the REM, may participate more directly in modulating Lte1 binding to Ras, with deregulated gain-of-function rendering the interaction constitutive, which in turn, abrogates checkpoint control.

The N-LRE includes a minimal CDK consensus site and three potential Cla4 sites (R-X-pS/T, Mok et al., 2010), yet, against expectations, we failed to detect phosphorylation by either CDK or Cla4 at those sequences *in vitro* (Figure 4). Whether our *in vitro* assay failed to reconstitute phosphorylation events that might otherwise occur *in vivo* at those sites remains unclear. However, the fact that $Lte1^{C-6D}$ expressed in a *cla4*Δ background retained compartmentalized localization to the bud and hyper-phosphorylation, suggested that additional protein kinases that might target the N-LRE to modulate binding to Ras might be also enriched at sites of polarized growth. This led us to the identification of Kin2, one of a pair of redundant yeast MARK/PAR-1 kinases as a novel regulator of Lte1. Kin2 phosphorylation at N-LRE sites specifically enhanced the interaction between Lte1 and Ras-GTP *in vitro* (Figure 6 H). Accordingly, phospho-mimetic substitutions within a close match to the consensus site for Kin1/2 in the N-LRE directed Lte1 localization to the mother cell cortex (Figure 6 B). Taken together, our studies identify Kin1/2 as one of the protein kinases that directly modulates Lte1 binding to Ras through phospho-sites within the N-LRE.

The combination of substitutions precluding phosphorylation at the 12 sites studied here in combination with six previously characterized CDK sites along the central domain of full-length Lte1 (Jensen et al., 2002) disrupted the program of Lte1 localization. Lte1^{18A} underwent recruitment at bud emergence but cortical association was not efficiently maintained during bud growth, resulting in limited apical localization in large budded cells. The fact that the *lte1^{18A}* allele increased the duration of anaphase, suggested that the disrupted localization might compromise Lte1 function as a timely activator of mitotic exit. Indeed, *lte1^{18A}* rescued *lte1*Δ *spo12*Δ co-lethality, demonstrating that the mutant protein still retained functionality (Supplement to Figure 7 C).

In conclusion, the use of phospho-mimetic substitutions has demonstrated distinct contributions for the C-LRE and N-LRE in Cla4-mediated recruitment and Lte1-Ras complex formation, respectively. However, genetic analysis based on inactivation of phospho-sites pointed to a degree of redundancy in the program. The failure to fully recapitulate phenotypes observed upon kinase inactivation may be due to additional sites outside the N-LRE or C-LRE and thus, not characterized here. Furthermore, these protein kinases may act through other substrates adding cell cycle or cell polarity-dependent inputs. Such multi-layered control and the apparent redundancy built into the program may contribute to the deployment of alternative cortical anchors for Lte1 according to developmental stage and cell cycle context. This flexibility may be also significant for Lte1 roles in MEN-independent control of cell polarity via the small GTPase Rsr1 (Geymonat et al., 2010).

Lte1 integrates spatial and temporal control using multisite phosphorylation

Multisite phosphorylation and cross-compartment signal propagation are recurrent themes in cell cycle control (Almawi et al., 2020; Jones et al., 2018; Miller and Turk, 2018; Ord et al., 2019; Rock et al., 2013; Zhou et al., 2021). When multiple protein kinases converge on a given substrate, their orderly activation might provide a phosphorylation timeline. In addition, interdependent phosphorylation events may occur when phospho-sites prime substrate recognition in a hierarchical manner. Phosphorylated residues by one kinase may be part of a consensus motif or may create docking sites on the substrate for the kinase that follows. Moreover, priming may impart a timeline for phosphorylation by driving substrate interaction with a scaffold protein or recruitment to a subcellular localization allowing for access to compartmentalized activation.

The inextricable relationship between Lte1 cortical association and phosphorylation has been attributed primarily to the interdependent relationship between Cla4 and Ras (Hofken and Schiebel, 2002; Seshan and Amon, 2005). In that view, local activation of Cdc42 and Cla4 singles out the incipient bud cortex for Lte1 binding to Ras, a small GTPase otherwise distributed over the entire cytoplasmic membrane.

Our findings suggest a more complicated set of partly redundant paths, given that multiple phospho-sites must be cancelled for substantial disruption of the program. This combinatorial input would set a strict temporal timeline subject to spatial constraints such that the ensuing association with Ras will not breach Lte1 compartmentalization or undermine SPOC proficiency.

In this model (Figure 8 C), Lte1 is effectively functioning as an integrator of multiple protein kinase inputs, with each kinase contributing temporal and/or spatial cues or even acting as coincidence detectors in their own right (as previously proposed for Cla4; Wild et al., 2004). G1-CDK would be the cell cycle trigger in this process (Jensen et al., 2002), Cla4 may provide a cortical tether (Seshan and Amon, 2005) and create a primed substrate as pre-requisites for Lte1 accessing locally active protein kinases enriched at sites of polarized growth like Kin1/2, perhaps acting in collaboration with mitotic-CDK and even mitotically active Cla4 (Benton et al., 1997). Conversely, conformational changes linked to membrane binding might provide a further feature for protein kinase access to intended target sites in Lte1, thus contributing to the observed interdependence between cortical association and phosphorylated status, even if the protein kinase is otherwise free to operate away from the cell cortex. Finally, the septin ring ensures a diffusion barrier for persistent compartmentalization (Castillon et al., 2003; Hofken and Schiebel, 2002; Jensen et al., 2002; Seshan et al., 2002). This series of events would permit and then reinforce Lte1-Ras complex formation only after a bud has formed, thus establishing and maintaining a bud cortical domain marked by an activator for timely mitotic exit. As a result, Lte1 is uniquely placed at the interface between cell cycle (Bardin et al., 2000; Pereira et al., 2000) and cell polarity (Geymonat et al., 2010) to enforce coordination between the two at the M/G1 transition.

An outstanding question is how this timeline of phosphorylation may be interlaced with control of protein-protein/protein-lipid interactions that may, transiently or in concert with Ras-GTP, support Lte1 polarized membrane association throughout the program. The observed Lte1 residual polarity in *ras1*Δ *ras2*Δ or *cla4*Δ cells may provide an indication of further redundancy that might involve known cortical partners

such as the small GTPase Rsr1 and the polarity determinant Kel1, both functionally significant interactors, even though neither appears to be absolutely essential for Lte1 program of localization (Geymonat et al., 2010; Hofken and Schiebel, 2002; Jensen et al., 2002; Seshan and Amon, 2005). It will be possible to dissect the molecular details of their various contributions and assign additional protein kinases targeting the N-LRE by exploiting the mutants generated in this study.

Ongoing developments in phospho-proteomics and computational approaches are set to accelerate the discovery of potential hubs linking small GTPase cascades, protein kinase networks and, perhaps most challenging, their substrates. At this global scale, new paradigms for integration between cell cycle and cell polarity control will emerge, although the need to dissect those in molecular detail remains, especially concerning phospho-targets. Our studies have uncovered a novel type of partnership subject to phospho-dependent control by which Lte1 is positioned to operate at the interface between different molecular switches due to its dual potential as effector (of Cdc42 and Ras) and regulator (of Rsr1 and Tem1), thus linking distinct small GTPase modules with cell cycle control. Furthermore, many of the components studied here are conserved in human cells in networks that control cell proliferation or cell polarity including PAKs, CDKs, MARK/PAR-1, Ras, Cdc42, and core components of the Hippo pathway (Chetty et al., 2022; Phillips et al., 2024; Sells and Chernoff, 1997; Wu and Griffin, 2017). For example, Cdc42-mediated polarity and the Hippo tumor-suppressor pathway (showing conservation with the MEN kinase core module) may be part of a functional axis for correct balance between the intestinal stem cell and the transit-amplifying pools that supports tissue homeostasis (Zhang et al., 2022). Also, cross-talk between Ras signaling and the Hippo pathway has significant implications in tumorigenesis (O'Neill, 2017). Given

the recognized relevance of these multiple players to proliferative disorders (Jang et al., 2020; Rane and Minden, 2019), achieving an integrative view, informed by studies in yeast, constitutes an important goal for uncovering new targets for therapeutic intervention.

MATERIALS AND METHODS

Yeast strains, constructs and genetic procedures

Yeast strains used in this study are listed in Supplementary Table 1. They were isogenic derivatives from 15DaubA *MAT***a** *bar1 ade1 his2 leu2-3,112 trp1-1a ura3Dns arg4* (Geymonat et al., 2020; Jensen et al., 2002; Juanes et al., 2013; Richardson et al., 1989), except when indicated otherwise. Yeast genetic procedures and media were according to Guthrie and Fink (1991). Rich medium (YEP) or synthetic medium with supplements, contained 2% w/v dextrose or 1% w/v sucrose according to the experiment. Induction of *GAL1*-driven expression was carried out in 1% w/v galactose as sole carbon source. Counter-selection of *URA3*-carrying plasmids was carried out in synthetic complete medium with 0.1% w/v 5-Fluoroorotic acid (5-FOA). Deletion of *LTE1, KIN1* and *KIN2* was carried out by one-step disruption using a targeted *KANMX* cassette produced by polymerase chain reaction. Alternatively, a *Hph* cassette was used when indicated (Geymonat et al., 2010). Deletion of *RAS1* and *RAS2* genes was carried out by one-step disruption using the insert from plasmid pRA545 (Tatchell et al., 1984) and a targeted *TRP1* cassette produced by polymerase chain reaction, respectively. One-step disruption of *BCY1* was carried out using a targeted *ADE1* cassette. pHIS2-P_{PGK1}-H-Ras was derived from pYGA-Ras (Clark et al., 1985). Strains expressing a GFP-Tub1 (yeast alpha-tubulin) fusion were created by transformation with pOB1 previously linearized with *Bsu*36I for integration at *TRP1* (Ten Hoopen et al., 2012).

Wild type *LTE1* or mutated versions encoding substitutions that either cancelled (S/T to A) or mimicked (S/T to D) phosphorylation at sites selected for study, were

generated by nested PCRs. The resulting ORFs were inserted as 4.3 kb *Sal*I-*Not*I fragments to generate in-frame fusions to GFP expressed under the control of the *HIS3* promoter into YIplac128. This plasmid series was used for transformation of a *lte1*Δ strain after linearization with *Bst*EII for integration at *LEU2*. Expression levels monitored by western blot analysis were found to be comparable for all mutants (Supplement to Figure 1 B). A modification of the intergenic flip flop one-step method (Mallet and Jacquet, 1996) was used to generate strains expressing $LTE1^{WT}$ or mutated versions fused to a protein A (ProA) tag under the control of the endogenous *LTE1* promoter.

Digital imaging microscopy

Early-log cultures grown at 23 °C in synthetic complete medium supplemented with 0.1 g/L adenine were concentrated by centrifugation at 380 x g for 5 min and directly spotted onto slides for still-image acquisition of random fields of cells with a Nikon Eclipse E800 with a CFI Plan Apochromat 100x, NA 1.4 objective, a Chroma Technology GFP filter set and a Coolsnap-HQ CCD camera (Roper Scientific), controlled by MetaMorph software (Molecular Devices). Single DIC images at the middle focal plane were paired to 5-plane Z-stacks of fluorescence images obtained at 0.8 µm intervals between planes with 2 x 2 binning (Guo and Segal, 2017). Representative images were selected from maximal intensity projections obtained with the open-source program FIJI (Schindelin et al., 2012). After adjusting consistently brightness and contrast, and scaling to 8-bit image depth, cell images were incorporated into final figures using Adobe Illustrator.

Time lapse recordings were performed by mounting cells from logarithmic cultures in complete synthetic dextrose containing 25 % w/v gelatin. 5-Z fluorescence image stacks paired to a transmitted light image at the middle focal plane were acquired at 1- or 2-min intervals using a modified Nikon Eclipse E800 fitted with OptoLED heads (Cairns Research) and Chroma Technology filter sets, a CFI Plan Apochromat 100x, NA 1.4 objective, a Z-focus drive and an Orca-Flash 4.0 v2 CMOS camera (Hamamatsu), all controlled by MetaMorph software (Guo and Segal, 2017).

Measurements were performed using FIJI plugins on maximal intensity projections after subtracting image background. Linescans for Lte1-GFP fluorescence intensity along the cell polarity (mother-bud) axis were generated with the line tool set to 5-pixel width. Gaussian fit of the resulting profile peaks was used to derive one-dimensional mean integrated intensity and peak width at half maximal intensity in individual budded cells paired to the length of the bud axis independently measured in DIC images with the line tool. Values were imported into Microsoft Excel for plotting. Smoothed conditional mean plots with 95% CI were generated using the open-source package R and the function geom_smooth (method = loess). Additionally, linescan datasets were ordered by measured bud size and grouped at 0.5 µm intervals between 1 ± 0.25 µm and 4.5 ± 0.25 µm. Traces in each group were realigned with respect to the position of the bud neck for averaging. Modes of Lte1-GFP cortical label were scored in still images of random fields of cells according to the categories outlined in Supplements to Figures 1 and 3. Data corresponded to the mean of three independent counts of at least 120 cells. Quantification of Lte1-GFP mean label intensity in time lapse series was carried out on maximal intensity projections by generating a binary mask in order to segment cortical label over the

entire bud. The resulting regions of interest were reviewed and, if necessary, edited manually. Measurements were collated for plotting in Microsoft Excel.

The mitotic spindle was visualized by still-imaging or time lapse using cells expressing GFP-Tub1. The distribution of budded cells according to mitotic spindle stage was scored in maximal intensity projections of still-images for random fields of asynchronous cells obtained as outlined above. Spindle stages in budded cells were categorized as follows: a) unseparated spindle poles (single focus of label associated with cytoplasmic microtubules); b) short spindles (from spindle pole separation to 2.5-µm long spindle); c) elongated spindles (> 2.5 µm long to fully elongated). The duration of anaphase B was determined in time lapse series as the interval from onset of the fast phase of spindle elongation until the last plane in which the elongated spindle was intact. Cells that did not reach spindle disassembly within the recorded time were not included.

$Lte1_{REM\text{-}CHD}$ model

Lte1 (residues 1-185 and 1190-1435) with two molecules of Ras1 (residues 8-174) were modelled based on the Ras-Sos1 complex (PDB 1nvv) with *Modeller* V9.20 (Sali and Blundell, 1993) and using slow loop refinement.

Protein production and purification

Recombinant MBP fusions to full-length or Lte1 fragments of wild type or phospho-site mutant versions were expressed and purified from yeast using an auto-selection expression system (Geymonat et al., 2007). Briefly, PCR cassettes encoding the relevant ORF flanked by homologous sites to the ends of gapped pMG3 expression vector were used for transformation of the host MGY853 (*MAT a ura3-1 trp1-28 leu2Δ0 lys2 his7 cdc28::LEU2 pep4::LEU2 [URA3-CDC28])* by gap-repair. Transformants were plated on 5-FOA to counter-select the resident *CDC28*-carrying plasmid. From that point, the expression construct was maintained in rich medium allowing for efficient protein expression. The strains used for expression of MBP-Lte1 fusion constructs are included in Supplementary table 1.

Protein induction was carried out in YEP-galactose for 8 hours at 30 °C. Cells were harvested, rinsed with ice-cold water, snap-frozen and stored at -80 °C. Pellets were resuspended to 1/20 volume of the original cell culture in cold breaking buffer (50 mM Tris-HCl pH 7.5, 250 mM NaCl, 0.2% NP-40, 10% v/v glycerol, 5 mM EDTA, Roche cOmplete-EDTA free protease inhibitor, 2mM PMSF, 5 mM DTT) and disrupted in a FastPrep-24™ grinder (MP Biomedicals) using 0.5-mm glass beads. Cell lysates were cleared by two cycles of centrifugation at 16,000 x g for 5 min at 4 °C. Amylose resin (New England Biolabs) was added and allowed to bind for 2 h on a rotator at 4 °C. The bound amylose resin was washed 6 times with washing buffer (50 mM Tris-HCl pH 7.5, 250 mM NaCl, 0.2% NP-40, 1 mM DTT) and once with 50% v/v glycerol in PBS. A ~500 µL slurry of bound resin in 50% v/v glycerol in PBS was stored at -20 °C. A 20 µL aliquot was resolved by SDS-PAGE and bound protein quantified by Coomassie blue staining against a BSA standard curve.

Purification of constitutively active Ras-GTP used in pull-down assays *in vitro* was undertaken using plasmid pMH919 encoding His_6-H-Ras^{V12}-myc-His_6 (strain MGY905, Supplementary table 1). As expression of $Ras2^{V19}$ was incompatible with the *GAL* induction protocol applied here, we took advantage of the fact that H-*ras* can fully replace yeast *RAS* genes for Lte1 localization (Supplement to Figure 2). The purification of the His-tagged protein was carried out following the above steps but using a different breaking buffer (50 mM Tris-HCl pH 7.5, 250 mM NaCl, 0.2% NP-40, 10% v/v glycerol, 20 mM imidazole, 5 mM β-ME, Roche cOmplete-EDTA free protease inhibitor, 2 mM PMSF), nickel resin (Super Ni-NTA Affinity Resin, Generon, #NB-45-00042-25) and washing buffer (50 mM Tris-HCl pH 7.5, 250 mM NaCl, 0.2% NP-40, 40 mM imidazole), followed by addition of elution buffer (30 mM Tris-HCl pH 7.5, 200 mM NaCl, 200 mM imidazole) to the packed resin to release soluble Ras protein. Protein concentrations were measured with Bradford reagent, and the most concentrated aliquots were combined for overnight dialysis against buffer A (20 mM Tris-HCl pH 7.5, 150 mM NaCl, 10% v/v glycerol, 500 µM DTT). Dialyzed proteins were assessed by SDS-PAGE and final aliquots stored at -80 °C.

A $Clb2^{\Delta db}$ stabilized version of the mitotic cyclin Clb2 was produced as a FLAG-$Clb2^{\Delta db}$-Chitin-Binding Domain (CBD) fusion protein in the context of overexpressed analog-sensitive Cdc28-as/His_6-Cks1 (strain MGY1111, Supplementary table 1). The CBD/intein tag enabled one-step purification by binding to chitin-resin (New England Biolabs) followed by elution of the CDK-as complex after inducible cleavage of the tag in 100 mM DTT at 4 °C.

Purification of the GST-tagged proteins GST-Cla4, GST-$Cla4^{KD}$ (K594A; Tjandra et al., 1998), GST-Kin2 and GST-$Kin2^{KD}$ (D248A; Ghosh et al., 2018) using glutathione

beads was carried out as previously described (Geymonat et al., 2009). Resin-bound fractions were stored in 50% v/v glycerol in 1x PBS at -20 °C. Alternatively, proteins were eluted with 20 mM reduced glutathione and dialyzed overnight at 4 °C in buffer A.

Western blot analysis, kinase and binding assays

Expression level of wild type Lte1-GFP or mutant versions was determined by western blot analysis of whole cell extracts resolved in an 8% SDS-PAGE gel as previously described (Ten Hoopen et al., 2012). GFP-tagged proteins were detected with a mouse monoclonal anti-GFP antibody mix (clones 7.1 and 13.1; Roche, used at 1:1000 dilution) and α-tubulin as loading control with monoclonal antibody B-5-1-2 (Sigma) used at 1:2000 dilution. Myc-tagged proteins were detected using mouse monoclonal 9E10 anti-Myc (Sigma) and His_6-tagged fusions were detected with anti-His mouse monoclonal antibody (Novagen) at 1:1000 dilution. For detection by chemiluminescence using goat anti-mouse HRP-conjugated secondary antibody (Invitrogen, Fisher scientific), blots were exposed to film or imaged in an Odyssey XF Imaging System (LI-COR Biosciences) in the chemiluminescence channel. For quantitative analysis the secondary antibody was goat anti-mouse IgG H&L (IRDye® 680RD) and the blot was imaged in the 700 nm channel of the Odyssey Imaging System.

Lte1 mobility shift reflecting bulk phosphorylation *in vivo* was assessed by western blot analysis of TCA whole extracts from cells expressing Lte1-ProA fusions at endogenous level. Briefly, early log YEP-dextrose cultures were synchronized in the

presence of 15 µg/mL nocodazole for 2.5 h at 25 °C and harvested by centrifugation. After washes in 1 mL cold H_2O and 1 mL 20% TCA, cells were re-suspended in 200 µL 20% TCA and disrupted with glass beads in a FastPrep-24™ grinder followed by addition of 400 µL 5% TCA and a further round of disruption. Lysates were collected and centrifuged for 10 min at 16,000 x g. The resulting pellet was re-suspended in 200 µL 2.5x Laemmli buffer and 50 µL 1M Tris base. Samples were heated at 95 °C for 5 min and subjected to 6% SDS-PAGE followed by western blot analysis. Direct detection of Lte1-ProA constructs was carried out with PAP (peroxidase anti-peroxidase) antibody (Sigma-Aldrich) used at 1:500 dilution.

Coimmunoprecipitation of wild type or mutant Lte1-ProA/His_6-Ras2 complexes was carried out in a 200-µL reaction containing 3 mg of whole cell extract, 30 µL of rabbit IgG agarose beads in 50 mM Tris-HCl pH 7.5, 150 mM NaCl, 1% NP-40, 1 mM DTT, incubated at 4 °C for 2 h. After extensive washing, beads were resuspended in 60 µL 2.5 x Laemmli buffer and placed 5 min at 95 °C followed by 10% SDS-PAGE and western blot analysis.

Protein kinase assays with purified components were carried out as follows. The kinase reaction contained 4 to 5 µg of MBP-Lte1 substrates bound to amylose beads, 40 µM ATP, 2 µCi [γ-^{32}P] ATP (3000 mCi/mmol; 10mCi/mL, Perkin-Elmer) and 15 to 25 ng of purified kinase in kinase buffer (50 mM Hepes pH 7.5, 10 mM $MgCl_2$, 2 mM $MnCl_2$ and 1 mM DTT) in a final volume of 30 µL. After a 30 min incubation at 30 °C with gentle tapping to maintain the beads suspended, reactions were stopped by addition of 10 µL of 5x Laemmli buffer and incubation at 95 °C for 3 min. 20 µL aliquots of the phosphorylation reaction were analyzed on an 8% SDS-PAGE gel. Gel was stained with InstantBlue Coomassie solution (Abcam), dried on

3MM blotting paper and exposed for up to 18 hours. The kinases assayed were GST-Cla4, GST-Cla4^{KD}, GST-Kin2, GST-Kin2^{KD} and Clb2/Cdc28-as. When indicated, Cdc28-as was inhibited by addition of 5 µM 1NM-PP1 (Geymonat et al., 2020).

In vitro pull-down reactions containing ~10 µg MBP-Lte1 versions bound to amylose resin and 5 µg soluble H-Ras^{V12}-myc in 300 µL binding buffer (50 mM Tris-HCl pH 7.5, 150 mM NaCl, 0.2% NP-40, 1 mg/mL BSA, 2 mM DTT) were incubated for 2 hours with rotation at 4 °C. After 6 washes with washing buffer (50 mM Tris-HCl pH 7.5, 200 mM NaCl, 0.2% NP-40, 2 mM DTT) the resin was resuspended in 60 µL Laemmli buffer and boiled for 4 min. Pull-down products were resolved on a 10% SDS-PAGE gel. The upper part of the gel (>37kDa) was stained in Coomassie Blue solution for 1 hour and destained overnight to visualize the bait. The lower part of the gel was analyzed by immunoblotting to assess H-Ras^{V12}-myc presence using monoclonal 9E10 anti-myc primary antibody. Imaging and quantification were carried out using the Odyssey Imaging System.

For pull-down assays preceded by phosphorylation, 7.5 µg of MBP-Lte1 proteins bound to amylose resin were incubated for 2 h at 37 °C with rotation in a 100 µL reaction containing 1 mM ATP, 50 ng of soluble GST-Kin2 or GST-Kin2^{KD} in kinase buffer (50 mM Hepes pH 7.5, 10 mM $MgCl_2$, 2 mM $MnCl_2$ and 1 mM DTT). Reactions were stopped by 2 washes of the resin with ice-cold washing buffer. Beads were then resuspended in 300 µL of binding buffer containing 5 µg soluble H-Ras^{V12}-myc and incubated with rotation at 4 °C for 2 h. Bound resin was washed 6 times with washing buffer, resuspended in 60 µL Laemmli buffer and boiled for 4 min before resolving by SDS-PAGE as described above.

ACKNOWLEDGEMENTS

We thank Olivia Edwards for contributing data to this project. Research reported in this publication was supported, in part, by the Department of Genetics, University of Cambridge (to MS), by a Herchel Smith Scholarship (to SP) and by CSC Cambridge International Scholarships (to QP). The authors declare no competing financial interests.

FIGURE LEGENDS

Figure 1. Program of Lte1 cortical localization and its dependence on the p21-activated kinase Cla4

(A) Contribution of Cla4 to bulk phosphorylation of Lte1 assessed by western blot analysis of whole extracts of wild type vs *cla4*Δ cells expressing Lte1 fused to Protein A (ProA), synchronized by arrest at metaphase (left panel). Mobility shift was evaluated using intensity linescans along the direction of electrophoretic migration (right panel). Inactivation of Cla4 virtually abrogated the phospho-dependent mobility shift as previously reported (Hofken and Schiebel, 2002; Seshan et al., 2002). (B) Fluorescence images selected from asynchronous populations representing stages for Lte1-GFP localization along the cell cycle in otherwise wild type vs *cla4*Δ cells. Scale bar, 2 µm. Expression levels of Lte1-GFP in the strains analyzed are presented in Supplement to Figure 1 B. (C) Modes of Lte1 localization in wild type vs *cla4*Δ budded cells scored collectively in still images from asynchronous populations. The plot presents the mean of 3 independent counts of 120 cells ± SEM. The categories scored are illustrated in Supplement to Figure 1 C. (D) Scatterplot (left) and smoothed conditional mean plot (right) for single-cell analysis of Lte1-GFP cortical spread along the bud cell polarity axis and mean intensity in the bud as a function of bud length in wild type (n = 258) vs *cla4*Δ (n = 223) cells, derived from fluorescence image linescans as described in Materials and Methods. Solid lines correspond to the smoothed conditional mean (locally weighted scatterplot smoothing) and shading represents the 95% CI. Distribution of bud length in each sample is presented in Supplement to Figure 1 D.

Supplement to Figure 1. Validating quantitative still imaging analysis of Lte1 cortical localization program

(A) Lte1 wild type program of cortical localization viewed by time lapse analysis at 21 ^{o}C. Top panel, selected frames from a time lapse series depicting initial accumulation of Lte1-GFP at the incipient bud (0), progressive cortical spreading during bud growth (24-125), delocalization at mitotic exit with slight localization at the division site (135-159), formation of a label crescent in the daughter cell (159-170) and the initiation of label at a new budding site in the former mother cell (170-onwards) followed later by the accumulation of Lte1 at the new budding site in the former daughter cell (215). Numbers indicate time elapsed in min. Scale bar, 2 µm. Bottom left panel, cartoon depicting the stages of Lte1 cortical localization with colored arrows matching the corresponding section of the plot quantifying mean fluorescence intensity as a function of time elapsed (bottom right panel). Mean fluorescence intensity was maximal shortly after bud emergence and decreased with spreading at the bud cortex during bud growth. This profile is consistent with single cell analysis in cell populations presented in Figure 1 D. (B) Lte1-GFP expression levels assessed by western blot analysis of whole cell extracts of strains used in live imaging studies. Tub1 was used as loading control. (C) Representative modes of Lte1 localization tallied in cell populations in Figures 1 C, 2 C and 2 F. (D) Cumulative distributions of bud length in asynchronous cell populations of wild type vs *cla4*Δ cells quantified in Figure 1 D. (E) Mean fluorescence intensity linescans (solid lines) ± SD (shaded area) compiled from the same dataset analyzed in Figure 1 D, according to bud length (± 0.25 µm). Note that fluorescence in the mother compartment reflects excess background of dispersed Lte1-GFP in the *cla4*Δ mutant.

Figure 2. Lte1 sequence requirements for phospho-dependent cortical localization

(A) Diagram outlining a minimal construct retaining Lte1 cortical localization. Sequences in Lte1$^{\Delta 250\text{-}950}$ adjacent to the REM (green box) and CHD (orange box), respectively, were required. (B) Representative images for Lte1$^{\Delta 250\text{-}950}$-GFP expressed in wild type vs *cla4*Δ cells. Lte1$^{\Delta 250\text{-}950}$ retained cortical localization dependent on Cla4. Scale bar, 2 µm. (C) Distribution of modes of Lte1$^{\Delta 250\text{-}950}$-GFP cortical localization in budded cells (as defined in Supplement to Figure 1 C) in otherwise wild type or *cla4*Δ mutant backgrounds. The plot shows the mean ± SEM of three independent counts of 120 cells. (D) Strategy for identifying critical residues in the putative REM of Lte1 that may be required for interaction with Ras-GTP. Modeled structure of an Lte1$_{\text{REM-CHD}}$ unit based upon hSOS1$_{\text{REM-CHD}}$ pinpointed V^{102} and R^{103} (blue) as counterparts of key residues in hSOS1 (red) required for Ras-GTP ("Ras allosteric") interaction with the REM (Sondermann et al., 2004). The mutant encoding V102E and R103A substitutions was referred to as *lte1^{mREM}*. (E) Representative fluorescence images for localization of Lte1^{WT}-GFP vs Lte1^{mREM}-GFP. Cortical localization was markedly reduced by substitutions within the putative REM and limited to subtle apical retention. Scale bar, 2 µm. (F) Distribution of modes of Lte1^{WT} vs Lte1^{mREM} cortical localization in budded cells. The plot shows the mean ± SEM of three independent counts of 120 cells. (G) Western blot analysis of whole cell extracts of the indicated strains following synchronization at metaphase (upper panel), paired with intensity linescans along the direction of electrophoretic migration (lower panel). Bulk phosphorylation of Lte1^{mREM} was markedly decreased and further reduced in a *cla4*Δ background. (H) Impaired suppression of *lte1*Δ *spo12*Δ synthetic lethality by *lte1^{mREM}*. *lte1*Δ *spo12*Δ *[URA3-SPO12]* cells transformed with integrative

plasmids encoding *LTE1* or *lte1*^{mREM} were spotted onto YEPD or 5-FOA plates to assess the ability of the integrative constructs to support viability upon counter-selection of the resident *URA3-SPO12* autonomous plasmid.

Supplement to Figure 2. H-Ras supports Lte1 localization in the absence of yeast Ras proteins

(A) Representative images for Lte1^{WT}-GFP localization in r*as1*Δ *ras2*Δ *bcy1*Δ *[*H-*ras]* vs *ras1*Δ *ras2*Δ *bcy1*Δ cells. Cells expressing H-Ras efficiently localized Lte1^{WT}-GFP. By contrast, cells lacking a Ras protein exhibited limited apical signal over increased cytoplasmic background. Scale bar, 2 µm. N.B. *bcy1*Δ is introduced to suppress *ras1*Δ *ras2*Δ lethality. (B) Distribution of modes of Lte1^{WT} localization collectively scored in budded cells of the indicated strains. The plot shows the mean ± SEM of three independent counts of 120 cells.

Figure 3. A cluster of phospho-sites proximal to the REM constitutes a regulatory element of Lte1's cortical program

(A) Diagram outlining the position and sequence of the N-terminal Lte1 regulatory element (N-LRE). Phospho-sites as curated by the SGD and selected for genetic analysis are shown in red. Also shown is a summary of substitutions created and product designation for the purpose of this study. (B) Phospho-mimetic substitutions directed Lte1 to the mother cell cortex, thus breaching Lte1 correct compartmentalization. Distribution of modes of Lte1-GFP localization scored in budded cells included two new categories — mother or mother and bud cell cortex (as illustrated in Supplement to Figure 3 A). The plot corresponds to mean ± SEM of three independent counts of at least 120 cells. (C) Localization of Lte1$^{N\text{-}4D}$ to the mother cell cortex (a-unbudded, b-small budded and c-large budded cells) persisted

in a *cla4*Δ mutant background (d) but was abrogated when further substitutions at the REM were introduced (e and f). Scale bar, 2 µm. (D) Distribution of modes of localization in budded cells of the indicated strains (according to the categories outlined in Supplement to Figure 3 A) showing mean ± SEM of three independent counts of at least 120 cells. (E) Western blot (upper panel) and intensity linescan analyses (lower panel) for Lte1 bulk phosphorylation assessed by mobility shift in whole extracts of cells expressing the indicated versions of Lte1-ProA in otherwise wild type or *cla4*Δ backgrounds prepared after synchronization at metaphase. Phospho-mimetic substitutions in the N-LRE restored Lte1 mobility shift, dependent on an intact REM, in a *cla4*Δ background. (F) Phospho-mimetic substitutions in the N-LRE enhanced Lte1's interaction with Ras-GTP in an *in vitro* pull-down assay. The indicated versions of Lte1 fused to MBP and H-Ras^{V12}-myc (an oncogenic mutant version that is constitutively bound to GTP, see Materials and Methods) were purified from yeast. After resolving the pull-down product by SDS-PAGE the lower part of the gel was excised and subjected to western blot analysis to visualize bound Ras while the top part was directly stained in Coomassie blue to view control MBP or MBP-Lte1 fusion baits. (G) Phospho-mimetic substitutions in the N-LRE also enhanced H-Ras^{V12}-myc binding to MBP-Lte1$^{\Delta 250\text{-}950}$ *in vitro*. Analysis of the pull-down was performed as in (F). (H) Phospho-mimetic substitutions within the N-LRE that disrupted Lte1 compartmentalization impaired the SPOC. Budded cells from cultures incubated at 14°C were scored using Spc29-CFP as a SPB marker according to the stages depicted in the cartoons (blue dots represent SPBs). In addition to cells containing unseparated SPBs (light blue), short spindles (red) and elongated spindles across the bud neck (yellow), a *dyn1*Δ mutation increased spindle misorientation, causing otherwise wild type cells to accumulate large-budded cells

with mispositioned anaphase spindles (green) in response to the SPOC. A *bfa1*Δ mutation abrogates the SPOC allowing cells to exit mitosis despite the presence of both spindle poles within the mother cell. This translates into an increase in cells undergoing re-budding and SPB re-duplication (violet). This latter category was also increased in $LTE1^{N\text{-}2D}$ and $LTE1^{N\text{-}4D}$ strains. The plot depicts the mean ± SEM of 3 independent counts of at least 120 cells. Representative images for each category scored are shown in Supplement to Figure 3 E. (I) Substitutions that cancel phosphorylation at the N-LRE abrogated rescue of *lte1*Δ *spo12*Δ synthetic lethality in the context of multicopy $lte1^{\Delta 250\text{-}950}$. *lte1*Δ *spo12*Δ *[URA3-SPO12]* cells transformed with the indicated integrative (YIp) or multicopy (2µm) plasmids were spotted onto YEPD or 5-FOA plates to assess viability upon counter-selection of the resident *URA3-SPO12* autonomous plasmid.

Supplement to Figure 3. Analysis of phospho-mimetic substitutions at the N-LRE

(A) Representative images for categories of cortical localization of Lte1 (as in Supplement to Figure 1 C) plus two further classes present in cells carrying phospho-mimetic substitutions at the N-LRE —mother cell cortex mainly (light blue) and mother and bud cell cortex (red). (B) Western blot and linescan analyses along the direction of electrophoretic migration of whole cell extracts of the indicated strains prepared after synchronization at metaphase. N-LRE phospho-mimetic mutants retained a mobility shift in a *cla4*Δ background. (C) Enhanced Lte1 binding to Ras caused by phospho-mimetic substitutions within the N-LRE. After resolving pulled-down products by SDS-PAGE, the top part of the gel was directly stained in Coomassie blue to view MBP-Lte1 baits while the bottom part was subjected to western blot analysis. (D) Mean Ras to Lte1 ratio in triplicate pull-downs ± SD. (E)

Representative images for the budded cell categories quantified in Figure 3 H. Unseparated SPBs (light blue), short spindles (red), elongated spindles across the bud neck (yellow), mispositioned anaphase spindles within the mother cell (green), cells undergoing rebudding with mispositioned spindles or further along the subsequent cell cycle following SPB reduplication (violet). Scale bar, 2 µm.

Figure 4. Failure of Cla4 and CDK to target the N-LRE *in vitro* pointed to further phosphorylation sites in a region near the CHD

(A-C) The N-LRE is not a prime target of Cla4 and CDK *in vitro*. (A) Deletion constructs used as kinase substrates. (B-C) *In vitro* kinase assay was carried out using the indicated substrates and either analogue-sensitive Clb2-Cdc28-as complex (CDK-as) or Cla4. After SDS-PAGE, the gel was stained with Coomassie blue and dried (lower panel) followed by exposure to film to detect radiolabeled species (upper panel). (B) Specific phosphorylation was detected on Lte1$^{1\text{-}325}$ fragment but phosphorylation was unaffected by substitutions that cancelled the studied phosphorylation sites at the N-LRE. An internally deleted Lte1 substrate essentially consisting of the REM and CHD (Lte1$^{\Delta 165\text{-}1144}$) showed reduced phosphorylation with either kinase. (C) Lte1$^{\Delta 250\text{-}950}$ was phosphorylated by CDK-as or Cla4 irrespective of substitutions cancelling phosphorylation at the N-LRE. Yet, a further deletion eliminating sequences adjacent to the CHD in Lte1$^{\Delta 250\text{-}1144}$ markedly reduced phosphorylation by both kinases. (D) Diagram outlining the position of regulatory sequences near the CHD. Phospho-sites annotated in the SGD and selected for genetic analysis are shown in red. Substitutions introduced in this study and their designation are indicated. The CHD-proximal cluster was referred to as the C-LRE here. (E-G) CDK and Cla4 target clusters of sites near the CHD (E) Deletion constructs used as kinase substrates. (F-G) *In vitro* kinase assays were performed

with the indicated substrates and enzymes. After SDS-PAGE, the gel was stained with Coomassie blue and dried (lower panel) followed by exposure to film to detect radiolabeled species (upper panel). (F) In the context of the indicated substrates, 6 S to A substitutions significantly reduced phosphorylation by either CDK or Cla4 *in vitro*. Combining those with substitutions within the N-LRE did not affect phosphorylation further. 1NM-PP1, inhibitory analog for CDK-as. KD, kinase dead version of Cla4. (G) By contrast, only Cla4 phosphorylation was markedly reduced when S^{1105}, S^{1109} and S^{1116} (C-3A; including one putative consensus for p21-activated kinase) were substituted to A.

Figure 5. Phospho-mimetic substitutions at the C-LRE restored correct Lte1 cortical localization in a *cla4*Δ background

(A) Representative fluorescence images for localization of $Lte1^{WT}$, $Lte1^{C\text{-}6D}$ or $Lte1^{C\text{-}3D}$ fused to GFP in a *cla4*Δ strain. Substitutions within the C-LRE rescued Lte1 localization in a *cla4*Δ background. Scale bar, 2 µm. (B-C) $LTE1^{C\text{-}3D}$ and $LTE1^{C\text{-}6D}$ suppressed the localization defect in a *cla4*Δ background to a comparable extent. (B) Distribution of modes of cortical localization in budded cells. The mean ± SEM for three independent counts of at least 120 cells is shown. (C) Scatterplot (left) and smoothed plot (right) for Lte1 cortical spread and mean intensity in the bud as a function of bud length in the indicated strains ($LTE1^{WT}$ *cla4*Δ n = 221, $LTE1^{C\text{-}6D}$ *cla4*Δ, n = 212, $LTE1^{C\text{-}3D}$ *cla4*Δ n= 203). Solid lines correspond to the smoothed conditional mean and shading represents the 95% CI. The cumulative distribution of bud length in the populations analyzed is shown in Supplement to Figure 5 B. (D) Impact of phospho-mimetic substitutions on Lte1's *in vivo* phosphorylation, assessed by western blot and linescan analyses. Whole extracts from the indicated strains were prepared after cell synchronization at metaphase. Phospho-mimetic

substitutions at the C-LRE significantly restored Lte1 mobility shift in a *cla4*Δ mutant background. Yet, a contribution of Cla4-dependent mobility remains, suggesting the presence of additional sites outside the C-LRE or an indirect contribution to the profile.

Supplement to Figure 5. Impact of phospho-mimetic substitutions at the C-LRE on Lte1 localization in *cla4*Δ cells

(A) Phospho-mimetic substitutions at the C-LRE do not perturb Lte1 compartmentalization to the bud. Representative images for Lte1$^{C\text{-}6D}$-GFP localization in otherwise wild type cells. Scale bar, 2 µm. (B) Cumulative distributions of bud length in still images of asynchronous cell populations quantified in Figures 5 C. (C) Mean fluorescence intensity linescans (solid lines) ± SD (shaded area) compiled from cells of the indicated bud length (± 0.25 µm) from the same dataset analyzed in Figure 5 C. Phospho-mimetic substitutions at the C-LRE restored Lte1 localization at the bud cell cortex in a *cla4*Δ mutant although the initial accumulation at the emerging bud did not reach wild type levels (compare with Supplement to Figure 1 E). Also note the suppression of excess cytoplasmic background label within the mother cell compartment relative to that observed for wild type Lte1 expressed in a *cla4*Δ background.

Figure 6. The MARK/PAR-1 like kinase Kin2 targets sites within the N-LRE

(A) N-LRE sequence outlining a potential site for MARK/PAR-1 like kinases. A PAK consensus site, 2 minimal Cla4 consensus sites (dotted line) and a minimal CDK consensus sites are also shown. (B) Phospho-mimetic substitutions at a putative target site for Kin1/2 protein kinase within the N-LRE (S219D-S222D) directed Lte1 to the mother cell cortex in unbudded (a) or budded (b) cells (left panel). Modes of

localization scored in budded cells for Lte1$^{N\text{-}4D}$-GFP vs Lte1^{219D,222D}-GFP (right panel). The plot shows mean ± SEM of three independent counts of at least 120 cells. Bias to the mother cell cortex was less pronounced for Lte1^{219D,222D} compared to Lte1$^{N\text{-}4D}$. (C) *In vitro* kinase assay was carried out using the indicated substrates and either purified Kin2 or Kin2 kinase-dead mutant (KD). After SDS-PAGE, the gel was stained with Coomassie blue and dried (lower panel) followed by exposure to film to detect radiolabeled species (upper panel). Substitutions that cancelled phosphorylation within the N-LRE reduced phosphorylation by Kin2 while Lte1$^{C\text{-}6A}$ was unaffected. (D) Impact of deletion of *KIN1* and *KIN2* on phospho-dependent mobility shift of Lte1-ProA vs Lte1$^{C\text{-}6A}$-ProA assessed by western blot (left panel) and linescan analyses (right panel). Extracts were prepared from cells synchronized at metaphase. Two exposures of the blot are shown. (E) Representative images for localization of Lte1$^{WT\text{-}GFP}$ in wild type (a-d) vs *kin1*Δ *kin2*Δ (e-h) budded cells. Scale bar, 2 µm. (F) Modes of Lte1^{WT}-GFP localization collectively scored in budded cells in otherwise wild type vs *kin1*Δ *kin2*Δ cells. Data corresponds to mean ± SEM for three independent counts of at least 120 cells. (G) Scatterplot (left) and smoothed plot (right) for Lte1^{WT} cortical spread and mean intensity in the bud as a function of bud length in otherwise wild type or *kin1*Δ *kin2*Δ backgrounds (*KIN1 KIN2* n = 259, *kin1*Δ *kin2*Δ n = 246). Solid lines correspond to the smoothed conditional mean and shading represents the 95% CI. Overall, cortical recruitment was reduced without otherwise preventing cortical spreading. (H) Phosphorylation by Kin2 enhanced Lte1's interaction with Ras-GTP *in vitro*, dependent on an intact N-LRE. MBP-Lte1^{WT} or MBP-Lte1$^{N\text{-}6A}$ were substrates for either mock (-) or Kin2 phosphorylation (+) reactions before incubation with purified H-Ras^{V12}-myc. A control reaction with a kinase-dead mutant version of Kin2 (KD) was included. After resolving pulled-down

products by SDS-PAGE the lower part of the gel was excised and subjected to western blot analysis to visualize bound Ras while the top part was directly stained in Coomassie blue to view MBP-Lte1 fusion baits.

Supplement to Figure 6. Contribution of Kin1/2 to the Lte1 program of cortical localization

(A) Phospho-mimetic substitutions at positions 219 and 222 markedly restored phospho-dependent mobility shift to Lte1 in a *cla4*Δ background, as assessed by western blot (upper panel) and linescan analyses along the direction of electrophoretic migration (lower panel). (B) Cumulative distributions of bud length in still images of asynchronous cell populations quantified in Figures 6 G. (C) Mean fluorescence intensity linescans (solid lines) ± SD (shaded area) compiled from cells of the indicated bud length (± 0.25 µm) from the same dataset analyzed in Figure 6 G. Overall Lte1 recruitment to the bud cell cortex was reduced in a *kin1*Δ *kin2*Δ background.

Figure 7. Cumulative effect of phospho-site substitutions on Lte1 cortical program

(A) Representative fluorescence images for localization of $Lte1^{WT}$, $Lte1^{12A}$ (see Figure 4D) and $Lte1^{18A}$ (additionally containing A substitutions at 6 previously identified CDK phosphorylation sites: T^{317}, T^{614}, S^{630}, S^{667}, T^{793} and S^{854}; Jensen et al., 2002) fused to GFP expressed in a wild type background. Scale bar, 2 µm. (B) Modes of Lte1 localization scored in budded cells for the same strains presented as mean ± SEM of three independent counts of at least 120 cells. (C) Scatterplot (left) and smoothed plot (right) for $Lte1^{WT}$-GFP, $Lte1^{12A}$-GFP and $Lte1^{18A}$-GFP cortical spread and mean intensity in the bud as a function of bud length in otherwise wild

type cells (*LTE1*^{WT} n = 272, *lte1*^{12A} n = 331, *lte1*^{18A} n= 283). Solid lines correspond to the smoothed conditional mean and shading represents the 95% CI. The cumulative distribution of bud lengths in each population is presented in Supplement to Figure 7 A. While Lte1^{12A} was not significantly affected, Lte1^{18A} was impaired for overall recruitment and progressively retained limited apical localization with bud growth. (D-E) *lte1*^{18A} cells exhibited a mitotic exit delay. (D) Distribution of budded cells along the spindle pathway assessed in still images from asynchronous populations of *LTE1* (n = 1509 cells) or *lte1*^{18A} (n = 1427 cells) strains. The *lte1*^{18A} strain showed a 27% increase in elongated-to-short spindle ratio, consistent with the lengthening of the anaphase interval. Error bars show 95% CI. ** $p<0.01$ according to the two proportion Z-test. (E) Mean duration of anaphase B was determined in *LTE1* (n = 30) vs *lte1*^{18A} (n = 21) cells by time lapse analysis as described in Materials and Methods. Error bars show SEM. ** $p<0.01$ according to the Mann Whitney two-tailed test.

Supplement to Figure 7. Further characterization of *lte1*^{18A}

(A) Cumulative distributions of bud length in the cell populations analyzed in Figures 7 C. (B) Mean fluorescence intensity linescans (solid lines) ± SD (shaded area) compiled from cells of the indicated bud length (± 0.25 µm) from the same dataset analyzed in Figure 7 C. (C) *lte1*^{18A} can suppress *lte1*Δ *spo12*Δ co-lethality as observed by the ability of transformants to grow upon counter-selection of the resident *URA3-SPO12* plasmid on 5-FOA medium.

Figure 8. Control of Lte1-Ras complex formation *in vivo* by N-LRE vs C-LRE

(A) *In vitro* pull-downs performed as described in Figure 3 F. After resolving the pull-down product by SDS-PAGE the lower part of the gel was excised and subjected to

western blot analysis to visualize bound Ras while the top part was directly stained in Coomassie blue to view control MBP or MBP-Lte1 fusion baits. Lte1's inherent ability to pull down Ras-GTP *in vitro* was unaffected by combining substitutions that cancel phosphorylation at N-LRE, C-LRE and CDK sites studied here. In addition, phospho-mimetic substitutions in $Lte1^{C\text{-}6D}$ did not enhance binding to Ras-GTP in contrast to the effect such substitutions had at the N-LRE (Figure 3 F). (B) *In vivo* interaction between Lte1 and Ras2 assessed by coimmunoprecipitation. Whole extracts were prepared from metaphase-arrested cells expressing the indicated versions of Lte1 fused to ProA and His_6-Ras2 replacing the respective endogenous loci in wild type or *cla4*Δ backgrounds. Co-precipitated Lte1 and Ras2 were analyzed by western blot. * MW standard reacted with anti-His antibody; ** IgG heavy chain cross-reacting band. (C) A model for multisite phosphorylation confining Lte1 to the bud cortical compartment. (a) In early G1, Lte1 is dephosphorylated and delocalized. G1-CDK (Cln-CDK) triggers passage through START. In turn, local activation of Cdc42 at the site selected for bud emergence dictates the recruitment of various polarity determinants including the PAK Cla4. Polarity factors and Cla4 may redundantly tether Lte1 while it undergoes phosphorylation at the C-LRE. These events would prime Lte1 recruitment to the incipient bud cell cortex. Kin1,2 enrichment at the emerging bud may also involve polarity factors such as Pea2 and Kel1 (Breitkreutz et al., 2010; Yuan et al., 2016). Whether Ras contributes at this stage of recruitment is unclear. (b) Following entry into S phase, Clb-CDK may target Kin1,2 and Cla4 (Holt et al., 2009; Lanz et al., 2021), thus contributing indirectly as well as directly to hyper-phosphorylation of primed Lte1 at and away from the N-LRE. This translates into Lte1 persistent association with Ras-GTP exclusively within the bud throughout the rest of the cell cycle. (c) Upon mitotic exit Lte1 dephosphorylation by Cdc14 and

PP2 phosphatases (Touati et al., 2019), reverses both binding to Ras and cortical association.

REFERENCES

Almawi, A.W., L. Langlois-Lemay, S. Boulton, J. Rodriguez Gonzalez, G. Melacini, D. D'Amours, and A. Guarne. 2020. Distinct surfaces on Cdc5/PLK Polo-box domain orchestrate combinatorial substrate recognition during cell division. *Sci. Rep.* 10:3379.

Anshu, A., M.A. Mannan, A. Chakraborty, S. Chakrabarti, and M. Dey. 2015. A novel role for protein kinase Kin2 in regulating HAC1 mRNA translocation, splicing, and translation. *Mol. Cell. Biol.* 35:199-210.

Bandaru, P., Y. Kondo, and J. Kuriyan. 2019. The Interdependent Activation of Son-of-Sevenless and Ras. *Cold Spring Harb. Perspect. Med.* 9:a031534.

Bardin, A.J., R. Visintin, and A. Amon. 2000. A mechanism for coupling exit from mitosis to partitioning of the nucleus. *Cell*. 102:21-31.

Baro, B., E. Queralt, and F. Monje-Casas. 2017. Regulation of Mitotic Exit in Saccharomyces cerevisiae. *Methods Mol. Biol.* 1505:3-17.

Benton, B.K., A. Tinkelenberg, I. Gonzalez, and F.R. Cross. 1997. Cla4p, a Saccharomyces cerevisiae Cdc42p-activated kinase involved in cytokinesis, is activated at mitosis. *Mol. Cell. Biol.* 17:5067-5076.

Bertazzi, D.T., B. Kurtulmus, and G. Pereira. 2011. The cortical protein Lte1 promotes mitotic exit by inhibiting the spindle position checkpoint kinase Kin4. *J. Cell Biol.* 193:1033-1048.

Bishop, A.C., J.A. Ubersax, D.T. Petsch, D.P. Matheos, N.S. Gray, J. Blethrow, E. Shimizu, J.Z. Tsien, P.G. Schultz, M.D. Rose, J.L. Wood, D.O. Morgan, and K.M. Shokat. 2000. A chemical switch for inhibitor-sensitive alleles of any protein kinase. *Nature*. 407:395-401.

Boguski, M.S., and F. McCormick. 1993. Proteins regulating Ras and its relatives. *Nature*. 366:643-654.

Bos, J.L., H. Rehmann, and A. Wittinghofer. 2007. GEFs and GAPs: critical elements in the control of small G proteins. *Cell*. 129:865-877.

Breitkreutz, A., H. Choi, J.R. Sharom, L. Boucher, V. Neduva, B. Larsen, Z.Y. Lin, B.J. Breitkreutz, C. Stark, G. Liu, J. Ahn, D. Dewar-Darch, T. Reguly, X. Tang, R. Almeida, Z.S. Qin, T. Pawson, A.C. Gingras, A.I. Nesvizhskii, and M. Tyers. 2010. A global protein kinase and phosphatase interaction network in yeast. *Science*. 328:1043-1046.

Broek, D., T. Toda, T. Michaeli, L. Levin, C. Birchmeier, M. Zoller, S. Powers, and M. Wigler. 1987. The S. cerevisiae CDC25 gene product regulates the RAS/adenylate cyclase pathway. *Cell*. 48:789-799.

Camonis, J.H., M. Kalekine, B. Gondre, H. Garreau, E. Boy-Marcotte, and M. Jacquet. 1986. Characterization, cloning and sequence analysis of the CDC25 gene which controls the cyclic AMP level of Saccharomyces cerevisiae. *EMBO J.* 5:375-380.

Casas Gimeno, G., and J. Paridaen. 2022. The Symmetry of Neural Stem Cell and Progenitor Divisions in the Vertebrate Brain. *Front. Cell Dev. Biol.* 10:885269.

Castillon, G.A., N.R. Adames, C.H. Rosello, H.S. Seidel, M.S. Longtine, J.A. Cooper, and R.A. Heil-Chapdelaine. 2003. Septins have a dual role in controlling mitotic exit in budding yeast. *Curr. Biol.* 13:654-658.

Caydasi, A.K., A. Khmelinskii, R. Duenas-Sanchez, B. Kurtulmus, M. Knop, and G. Pereira. 2017. Temporal and compartment-specific signals coordinate mitotic exit with spindle position. *Nat. Commun.* 8:14129.

Caydasi, A.K., and G. Pereira. 2009. Spindle alignment regulates the dynamic association of checkpoint proteins with yeast spindle pole bodies. *Dev. Cell*. 16:146-156.

Caydasi, A.K., and G. Pereira. 2012. SPOC alert--when chromosomes get the wrong direction. *Exp. Cell Res.* 318:1421-1427.

Chan, L.Y., and A. Amon. 2010. Spindle position is coordinated with cell-cycle progression through establishment of mitotic exit-activating and -inhibitory zones. *Mol. Cell*. 39:444-454.

Chetty, A.K., B.H. Ha, and T.J. Boggon. 2022. Rho family GTPase signaling through type II p21-activated kinases. *Cell. Mol. Life. Sci.* 79:598.

Chiou, J.G., M.K. Balasubramanian, and D.J. Lew. 2017. Cell Polarity in Yeast. *Annu. Rev. Cell Dev. Biol.* 33:77-101.

Clark, S.G., J.P. McGrath, and A.D. Levinson. 1985. Expression of normal and activated human Ha-ras cDNAs in Saccharomyces cerevisiae. *Mol. Cell. Biol.* 5:2746-2752.

D'Aquino, K.E., F. Monje-Casas, J. Paulson, V. Reiser, G.M. Charles, L. Lai, K.M. Shokat, and A. Amon. 2005. The protein kinase Kin4 inhibits exit from mitosis in response to spindle position defects. *Mol. Cell*. 19:223-234.

Elbert, M., G. Rossi, and P. Brennwald. 2005. The yeast par-1 homologs kin1 and kin2 show genetic and physical interactions with components of the exocytic machinery. *Mol. Biol. Cell*. 16:532-549.

Falk, J.E., I.W. Campbell, K. Joyce, J. Whalen, A. Seshan, and A. Amon. 2016a. LTE1 promotes exit from mitosis by multiple mechanisms. *Mol. Biol. Cell*. 27:3991-4001.

Falk, J.E., L.Y. Chan, and A. Amon. 2011. Lte1 promotes mitotic exit by controlling the localization of the spindle position checkpoint kinase Kin4. *Proc. Natl. Acad. Sci. U. S. A.* 108:12584-12590.

Falk, J.E., D. Tsuchiya, J. Verdaasdonk, S. Lacefield, K. Bloom, and A. Amon. 2016b. Spatial signals link exit from mitosis to spindle position. *eLife*. 5:e14036.

Fraschini, R., C. D'Ambrosio, M. Venturetti, G. Lucchini, and S. Piatti. 2006. Disappearance of the budding yeast Bub2-Bfa1 complex from the mother-bound spindle pole contributes to mitotic exit. *J. Cell Biol.* 172:335-346.

Geymonat, M., Q. Peng, Z. Guo, Z. Yu, J.R. Unruh, S.L. Jaspersen, and M. Segal. 2020. Orderly assembly underpinning built-in asymmetry in the yeast centrosome duplication cycle requires cyclin-dependent kinase. *eLife*. 9:e59222.

Geymonat, M., and M. Segal. 2017. Intrinsic and Extrinsic Determinants Linking Spindle Pole Fate, Spindle Polarity, and Asymmetric Cell Division in the Budding Yeast S. cerevisiae. *Results Probl. Cell. Differ.* 61:49-82.

Geymonat, M., A. Spanos, G. de Bettignies, and S.G. Sedgwick. 2009. Lte1 contributes to Bfa1 localization rather than stimulating nucleotide exchange by Tem1. *J. Cell Biol.* 187:497-511.

Geymonat, M., A. Spanos, S. Jensen, and S.G. Sedgwick. 2010. Phosphorylation of Lte1 by Cdk prevents polarized growth during mitotic arrest in S. cerevisiae. *J. Cell Biol.* 191:1097-1112.

Geymonat, M., A. Spanos, and S.G. Sedgwick. 2007. A Saccharomyces cerevisiae autoselection system for optimised recombinant protein expression. *Gene*. 399:120-128.

Geymonat, M., A. Spanos, S.J. Smith, E. Wheatley, K. Rittinger, L.H. Johnston, and S.G. Sedgwick. 2002. Control of mitotic exit in budding yeast. In vitro regulation of Tem1 GTPase by Bub2 and Bfa1. *J. Biol. Chem.* 277:28439-28445.

Geymonat, M., A. Spanos, P.A. Walker, L.H. Johnston, and S.G. Sedgwick. 2003. In vitro regulation of budding yeast Bfa1/Bub2 GAP activity by Cdc5. *J. Biol. Chem.* 278:14591-14594.

Ghosh, C., L. Sathe, J.D. Paprocki, V. Raicu, and M. Dey. 2018. Adaptation to Endoplasmic Reticulum Stress Requires Transphosphorylation within the Activation Loop of Protein Kinases Kin1 and Kin2, Orthologs of Human Microtubule Affinity-Regulating Kinase. *Mol. Cell. Biol.* 38:e00266-00218.

Ghosh, C., J.K. Uppala, L. Sathe, C.I. Hammond, A. Anshu, P.R. Pokkuluri, B.E. Turk, and M. Dey. 2021. Phosphorylation of Pal2 by the protein kinases Kin1 and Kin2 modulates HAC1 mRNA splicing in the unfolded protein response in yeast. *Sci. Signal*. 14:eaaz4401.

Guo, X., and J. Dong. 2022. Protein polarization: Spatiotemporal precisions in cell division and differentiation. *Curr. Opin. Plant Biol.* 68:102257.

Guo, Z., and M. Segal. 2017. Analysis of the localization of MEN components by live cell imaging microscopy. *Methods Mol. Biol.* 1505:151-166.

Guthrie, C., and G.R. Fink. 1991. Guide to yeast genetics and molecular biology. Academic Press, Inc., San Diego, CA.

Habib, S.J., and S.P. Acebron. 2022. Wnt signalling in cell division: from mechanisms to tissue engineering. *Trends Cell Biol.* 32:1035-1048.

Hofken, T., and E. Schiebel. 2002. A role for cell polarity proteins in mitotic exit. *EMBO J.* 21:4851-4862.

Holt, L.J., B.B. Tuch, J. Villen, A.D. Johnson, S.P. Gygi, and D.O. Morgan. 2009. Global analysis of Cdk1 substrate phosphorylation sites provides insights into evolution. *Science*. 325:1682-1686.

Hu, F., Y. Wang, D. Liu, Y. Li, J. Qin, and S.J. Elledge. 2001. Regulation of the Bub2/Bfa1 GAP complex by Cdc5 and cell cycle checkpoints. *Cell*. 107:655-665.

Jang, J.W., M.K. Kim, and S.C. Bae. 2020. Reciprocal regulation of YAP/TAZ by the Hippo pathway and the Small GTPase pathway. *Small GTPases*. 11:280-288.

Jaspersen, S.L., J.F. Charles, and D.O. Morgan. 1999. Inhibitory phosphorylation of the APC regulator Hct1 is controlled by the kinase Cdc28 and the phosphatase Cdc14. *Curr. Biol.* 9:227-236.

Jaspersen, S.L., J.F. Charles, R.L. Tinker-Kulberg, and D.O. Morgan. 1998. A late mitotic regulatory network controlling cyclin destruction in Saccharomyces cerevisiae. *Mol. Biol. Cell*. 9:2803-2817.

Jensen, S., M. Geymonat, A.L. Johnson, M. Segal, and L.H. Johnston. 2002. Spatial regulation of the guanine nucleotide exchange factor Lte1 in Saccharomyces cerevisiae. *J. Cell Sci.* 115:4977-4991.

Jensen, S., A.L. Johnson, L.H. Johnston, and M. Segal. 2004. Temporal coupling of spindle disassembly and cytokinesis is disrupted by deletion of LTE1 in budding yeast. *Cell Cycle*. 3:817-822.

Jeschke, G.R., H.J. Lou, K. Weise, C.I. Hammond, M. Demonch, P. Brennwald, and B.E. Turk. 2018. Substrate priming enhances phosphorylation by the budding yeast kinases Kin1 and Kin2. *J. Biol. Chem.* 293:18353-18364.

Jones, M.H., E.T. O'Toole, A.S. Fabritius, E.G. Muller, J.B. Meehl, S.L. Jaspersen, and M. Winey. 2018. Key phosphorylation events in Spc29 and Spc42 guide multiple steps of yeast centrosome duplication. *Mol. Biol. Cell*. 29:2280-2291.

Juanes, M.A., H. Twyman, E. Tunnacliffe, Z. Guo, R. ten Hoopen, and M. Segal. 2013. Spindle pole body history intrinsically links pole identity with asymmetric fate in budding yeast. *Curr. Biol.* 23:1310-1319.

Lanz, M.C., K. Yugandhar, S. Gupta, E.J. Sanford, V.M. Faca, S. Vega, A.M.N. Joiner, J.C. Fromme, H. Yu, and M.B. Smolka. 2021. In-depth and 3-dimensional exploration of the budding yeast phosphoproteome. *EMBO Rep*. 22:e51121.

Lee, S.E., S. Jensen, L.M. Frenz, A.L. Johnson, D. Fesquet, and L.H. Johnston. 2001. The Bub2-dependent mitotic pathway in yeast acts every cell cycle and regulates cytokinesis. *J. Cell Sci.* 114:2345-2354.

Levin, D.E., C.I. Hammond, R.O. Ralston, and J.M. Bishop. 1987. Two yeast genes that encode unusual protein kinases. *Proc. Natl. Acad. Sci. U. S. A.* 84:6035-6039.

Li, Y.Y., E. Yeh, T. Hays, and K. Bloom. 1993. Disruption of mitotic spindle orientation in a yeast dynein mutant. *Proc. Natl. Acad. Sci. U. S. A.* 90:10096-10100.

Mallet, L., and M. Jacquet. 1996. Intergenic Flip Flop, a method for systematic gene disruption and cloning in yeast. *Yeast*. 12:1351-1357.

Margarit, S.M., H. Sondermann, B.E. Hall, B. Nagar, A. Hoelz, M. Pirruccello, D. Bar-Sagi, and J. Kuriyan. 2003. Structural evidence for feedback activation by Ras.GTP of the Ras-specific nucleotide exchange factor SOS. *Cell*. 112:685-695.

Marquardt, J., X. Chen, and E. Bi. 2021. Septin Assembly and Remodeling at the Cell Division Site During the Cell Cycle. *Front. Cell Dev. Biol.* 9:793920.

Miller, C.J., and B.E. Turk. 2018. Homing in: Mechanisms of Substrate Targeting by Protein Kinases. *Trends Biochem. Sci*. 43:380-394.

Mok, J., P.M. Kim, H.Y. Lam, S. Piccirillo, X. Zhou, G.R. Jeschke, D.L. Sheridan, S.A. Parker, V. Desai, M. Jwa, E. Cameroni, H. Niu, M. Good, A. Remenyi, J.L. Ma, Y.J. Sheu, H.E. Sassi, R. Sopko, C.S. Chan, C. De Virgilio, N.M. Hollingsworth, W.A.

Lim, D.F. Stern, B. Stillman, B.J. Andrews, M.B. Gerstein, M. Snyder, and B.E. Turk. 2010. Deciphering protein kinase specificity through large-scale analysis of yeast phosphorylation site motifs. *Sci. Signal*. 3:ra12.

Monje-Casas, F., and A. Amon. 2009. Cell polarity determinants establish asymmetry in MEN signaling. *Dev. Cell*. 16:132-145.

O'Neill, E. 2017. Ras and the Hippo pathway in cancer. *In* Conquering Ras. Elsevier. 25-39.

Okada, S., M. Leda, J. Hanna, N.S. Savage, E. Bi, and A.B. Goryachev. 2013. Daughter cell identity emerges from the interplay of Cdc42, septins, and exocytosis. *Dev. Cell*. 26:148-161.

Ord, M., K. Moll, A. Agerova, R. Kivi, I. Faustova, R. Venta, E. Valk, and M. Loog. 2019. Multisite phosphorylation code of CDK. *Nat. Struct. Mol. Biol.* 26:649-658.

Pereira, G., T. Hofken, J. Grindlay, C. Manson, and E. Schiebel. 2000. The Bub2p spindle checkpoint links nuclear migration with mitotic exit. *Mol. Cell*. 6:1-10.

Pereira, G., and E. Schiebel. 2005. Kin4 kinase delays mitotic exit in response to spindle alignment defects. *Mol. Cell*. 19:209-221.

Pereira, G., T.U. Tanaka, K. Nasmyth, and E. Schiebel. 2001. Modes of spindle pole body inheritance and segregation of the Bfa1p-Bub2p checkpoint protein complex. *EMBO J.* 20:6359-6370.

Phillips, J.E., Y. Zheng, and D. Pan. 2024. Assembling a Hippo: the evolutionary emergence of an animal developmental signaling pathway. *Trends Biochem. Sci*. 49:681-692.

Pineau, J., H. Moreau, A.L. Dumenil, and P. Pierobon. 2023. Polarity in immune cells. *Curr. Top. Dev. Biol.* 154:197-222.

Queralt, E., and F. Uhlmann. 2008. Cdk-counteracting phosphatases unlock mitotic exit. *Curr. Opin. Cell. Biol.* 20:661-668.

Rane, C.K., and A. Minden. 2019. P21 activated kinase signaling in cancer. *Semin. Cancer Biol.* 54:40-49.

Richardson, H.E., C. Wittenberg, F. Cross, and S.I. Reed. 1989. An essential G1 function for cyclin-like proteins in yeast. *Cell*. 59:1127-1133.

Robinson, L.C., J.B. Gibbs, M.S. Marshall, I.S. Sigal, and K. Tatchell. 1987. CDC25: a component of the RAS-adenylate cyclase pathway in Saccharomyces cerevisiae. *Science*. 235:1218-1221.

Rock, J.M., and A. Amon. 2009. The FEAR network. *Curr. Biol.* 19:R1063-1068.

Rock, J.M., D. Lim, L. Stach, R.W. Ogrodowicz, J.M. Keck, M.H. Jones, C.C.L. Wong, J.R. Yates, M. Winey, S.J. Smerdon, M.B. Yaffe, and A. Amon. 2013. Activation of the Yeast Hippo Pathway by Phosphorylation-Dependent Assembly of Signaling Complexes. *Science*. 340:871-875.

Sali, A., and T.L. Blundell. 1993. Comparative protein modelling by satisfaction of spatial restraints. *J. Mol. Biol.* 234:779-815.

Scarfone, I., and S. Piatti. 2015. Coupling spindle position with mitotic exit in budding yeast: The multifaceted role of the small GTPase Tem1. *Small GTPases*. 6:196-201.

Sells, M.A., and J. Chernoff. 1997. Emerging from the Pak: the p21-activated protein kinase family. *Trends Cell Biol.* 7:162-167.

Seshan, A., and A. Amon. 2005. Ras and the Rho effector Cla4 collaborate to target and anchor Lte1 at the bud cortex. *Cell Cycle*. 4:940-946.

Seshan, A., A.J. Bardin, and A. Amon. 2002. Control of Lte1 localization by cell polarity determinants and Cdc14. *Curr. Biol.* 12:2098-2110.

Shirayama, M., Y. Matsui, K. Tanaka, and A. Toh-e. 1994a. Isolation of a CDC25 family gene, MSI2/LTE1, as a multicopy suppressor of ira1. *Yeast*. 10:451-461.

Shirayama, M., Y. Matsui, and E.A. Toh. 1994b. The yeast TEM1 gene, which encodes a GTP-binding protein, is involved in termination of M phase. *Mol. Cell. Biol.* 14:7476-7482.

Shou, W., J.H. Seol, A. Shevchenko, C. Baskerville, D. Moazed, Z.W. Chen, J. Jang, A. Shevchenko, H. Charbonneau, and R.J. Deshaies. 1999. Exit from mitosis is triggered by Tem1-dependent release of the protein phosphatase Cdc14 from nucleolar RENT complex. *Cell*. 97:233-244.

Sondermann, H., S.M. Soisson, S. Boykevisch, S.S. Yang, D. Bar-Sagi, and J. Kuriyan. 2004. Structural analysis of autoinhibition in the Ras activator Son of sevenless. *Cell*. 119:393-405.

Spiliotis, E.T., and M.A. McMurray. 2020. Masters of asymmetry - lessons and perspectives from 50 years of septins. *Mol. Biol. Cell*. 31:2289-2297.

Stegmeier, F., R. Visintin, and A. Amon. 2002. Separase, polo kinase, the kinetochore protein Slk19, and Spo12 function in a network that controls Cdc14 localization during early anaphase. *Cell*. 108:207-220.

Tatchell, K., D.T. Chaleff, D. DeFeo-Jones, and E.M. Scolnick. 1984. Requirement of either of a pair of ras-related genes of Saccharomyces cerevisiae for spore viability. *Nature*. 309:523-527.

Ten Hoopen, R., C. Cepeda-Garcia, R. Fernandez-Arruti, M.A. Juanes, N. Delgehyr, and M. Segal. 2012. Mechanism for astral microtubule capture by cortical Bud6p priming spindle polarity in S. cerevisiae. *Curr. Biol.* 22:1075-1083.

Tjandra, H., J. Compton, and D. Kellogg. 1998. Control of mitotic events by the Cdc42 GTPase, the Clb2 cyclin and a member of the PAK kinase family. *Curr. Biol.* 8:991-1000.

Touati, S.A., L. Hofbauer, A.W. Jones, A.P. Snijders, G. Kelly, and F. Uhlmann. 2019. Cdc14 and PP2A Phosphatases Cooperate to Shape Phosphoproteome Dynamics during Mitotic Exit. *Cell Rep*. 29:2105-2119 e2104.

Ubersax, J.A., E.L. Woodbury, P.N. Quang, M. Paraz, J.D. Blethrow, K. Shah, K.M. Shokat, and D.O. Morgan. 2003. Targets of the cyclin-dependent kinase Cdk1. *Nature*. 425:859-864.

Visintin, R., K. Craig, E.S. Hwang, S. Prinz, M. Tyers, and A. Amon. 1998. The phosphatase Cdc14 triggers mitotic exit by reversal of Cdk-dependent phosphorylation. *Mol. Cell*. 2:709-718.

Visintin, R., E.S. Hwang, and A. Amon. 1999. Cfi1 prevents premature exit from mitosis by anchoring Cdc14 phosphatase in the nucleolus. *Nature*. 398:818-823.

Wild, A.C., J.W. Yu, M.A. Lemmon, and K.J. Blumer. 2004. The p21-activated protein kinase-related kinase Cla4 is a coincidence detector of signaling by Cdc42 and phosphatidylinositol 4-phosphate. *J. Biol. Chem.* 279:17101-17110.

Wu, Y., and E.E. Griffin. 2017. Regulation of Cell Polarity by PAR-1/MARK Kinase. *Curr. Top. Dev. Biol.* 123:365-397.

Yamashita, Y.M. 2023. Asymmetric Stem Cell Division and Germline Immortality. *Annu. Rev. Genet.* 57:181-199.

Yoshida, S., R. Ichihashi, and A. Toh-e. 2003. Ras recruits mitotic exit regulator Lte1 to the bud cortex in budding yeast. *J. Cell Biol.* 161:889-897.

Yuan, S.M., W.C. Nie, F. He, Z.W. Jia, and X.D. Gao. 2016. Kin2, the Budding Yeast Ortholog of Animal MARK/PAR-1 Kinases, Localizes to the Sites of Polarized Growth and May Regulate Septin Organization and the Cell Wall. *PLoS One*. 11:e0153992.

Zhang, Z., F. Zhang, A.K. Davis, M. Xin, G. Walz, W. Tian, and Y. Zheng. 2022. CDC42 controlled apical-basal polarity regulates intestinal stem cell to transit amplifying cell fate transition via YAP-EGF-mTOR signaling. *Cell Rep*. 38:110009.

Zhou, X., W. Li, Y. Liu, and A. Amon. 2021. Cross-compartment signal propagation in the mitotic exit network. *eLife*. 10:e63645.

Zhou, X., S.Y. Weng, S.P. Bell, and A. Amon. 2024. A noncanonical GTPase signaling mechanism controls exit from mitosis in budding yeast. *Proc. Natl. Acad. Sci. U. S. A.* 121:e2413873121.

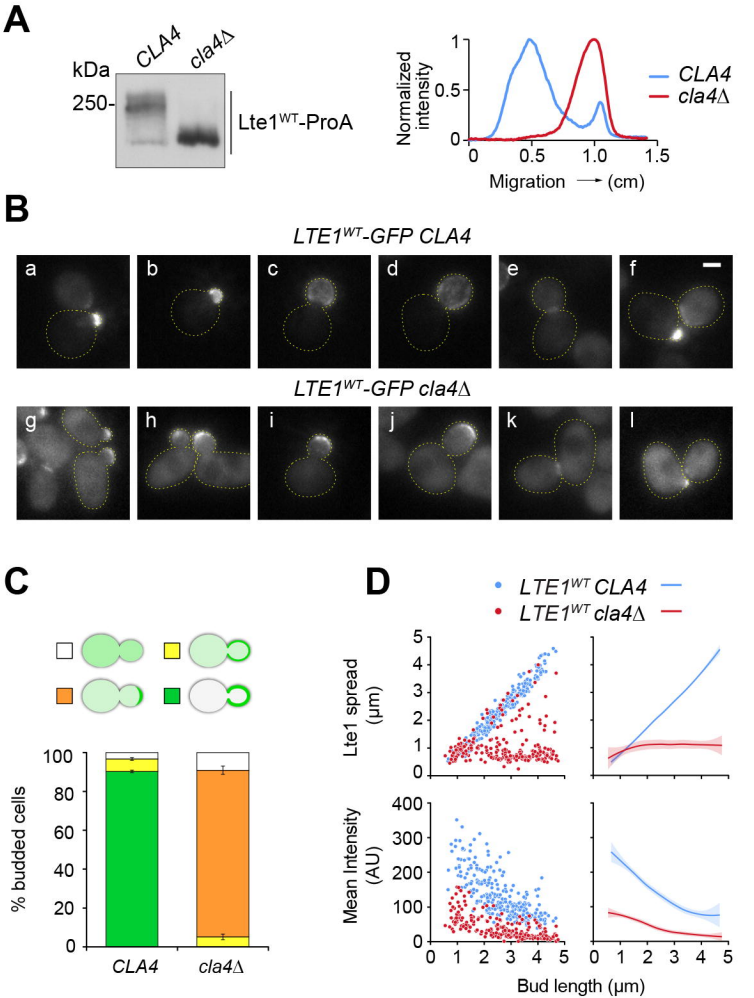
A
kDa
CLA4
cla4Δ
250-
Lte1WT-ProA
Normalized intensity
1
0.5
0
0
0.5
1.0
1.5
Migration → (cm)
CLA4
cla4Δ
B
LTE1WT-GFP CLA4
a
b
c
d
e
f
LTE1WT-GFP cla4Δ
g
h
i
j
k
l
C
% budded cells
100
80
60
40
20
0
CLA4
cla4Δ
D
LTE1WT CLA4
LTE1WT cla4Δ
Lte1 spread (µm)
Mean Intensity (AU)
Bud length (µm)

Fig1

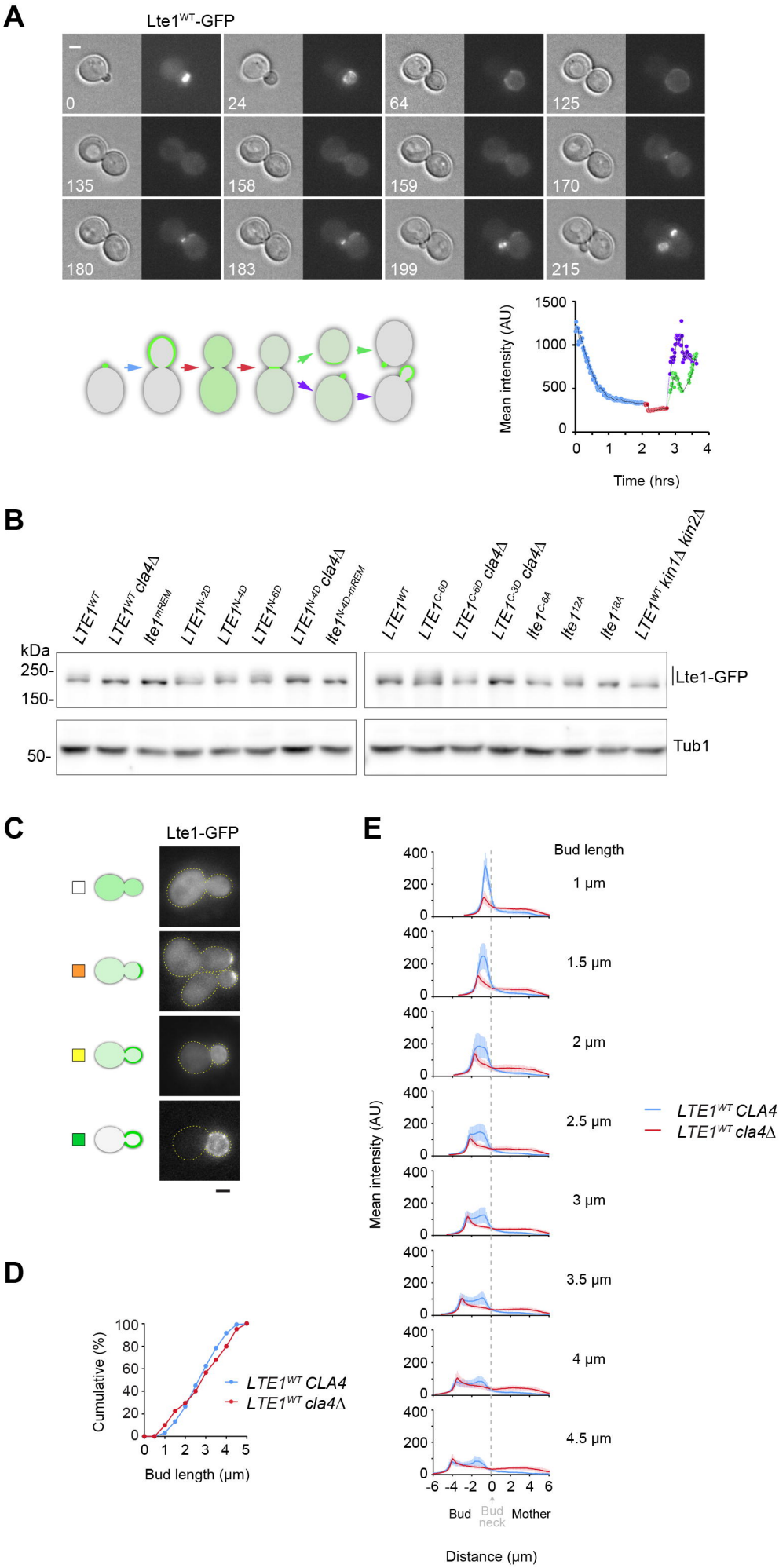

Suppl to Fig1

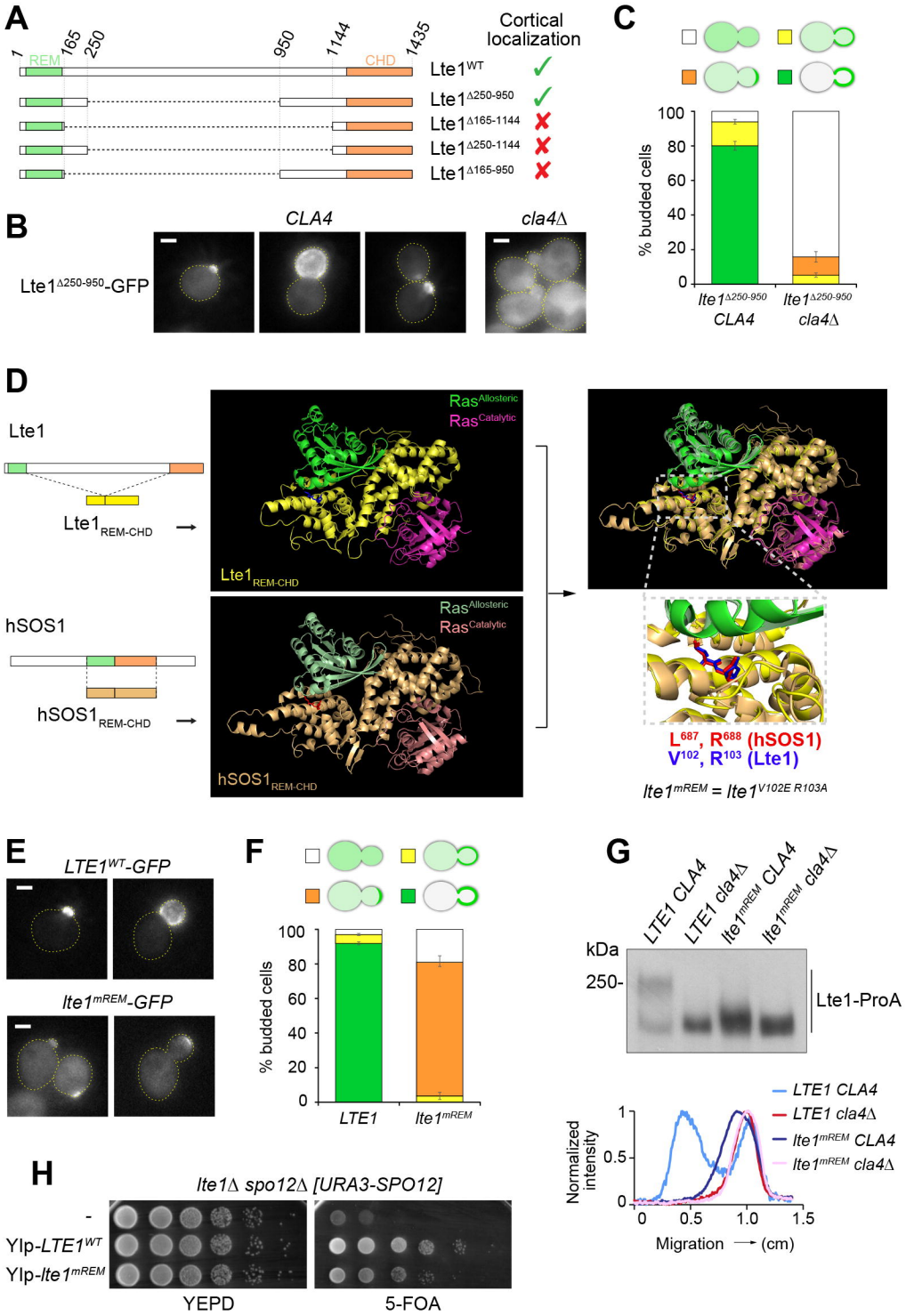
A
Cortical localization
1
165
250
950
1144
1435
REM
CHD
Lte1WT
Lte1Δ250-950
Lte1Δ165-1144
Lte1Δ250-1144
Lte1Δ165-950
B
CLA4
cla4Δ
Lte1Δ250-950-GFP
C
% budded cells
100
80
60
40
20
0
lte1Δ250-950
CLA4
cla4Δ
D
Lte1
Lte1REM-CHD
hSOS1
hSOS1REM-CHD
RasAllosteric
RasCatalytic
L687, R688 (hSOS1)
V102, R103 (Lte1)
lte1mREM = lte1V102E R103A
E
LTE1WT-GFP
lte1mREM-GFP
F
% budded cells
LTE1
lte1mREM
G
LTE1 CLA4
LTE1 cla4Δ
lte1mREM CLA4
lte1mREM cla4Δ
kDa
250-
Lte1-ProA
Normalized intensity
Migration (cm)
H
lte1Δ spo12Δ [URA3-SPO12]
-
YIp-LTE1WT
YIp-lte1mREM
YEPD
5-FOA

Fig2

A

Lte1^{WT}-GFP

ras1Δ ras2Δ bcy1Δ [H-ras]

ras1Δ ras2Δ bcy1Δ

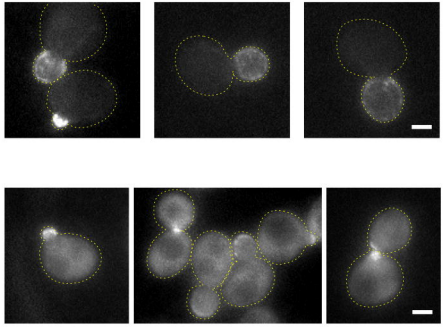

B

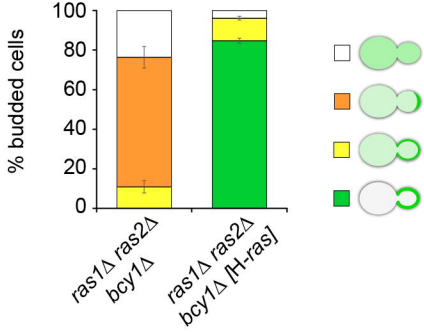

Suppl to Fig2

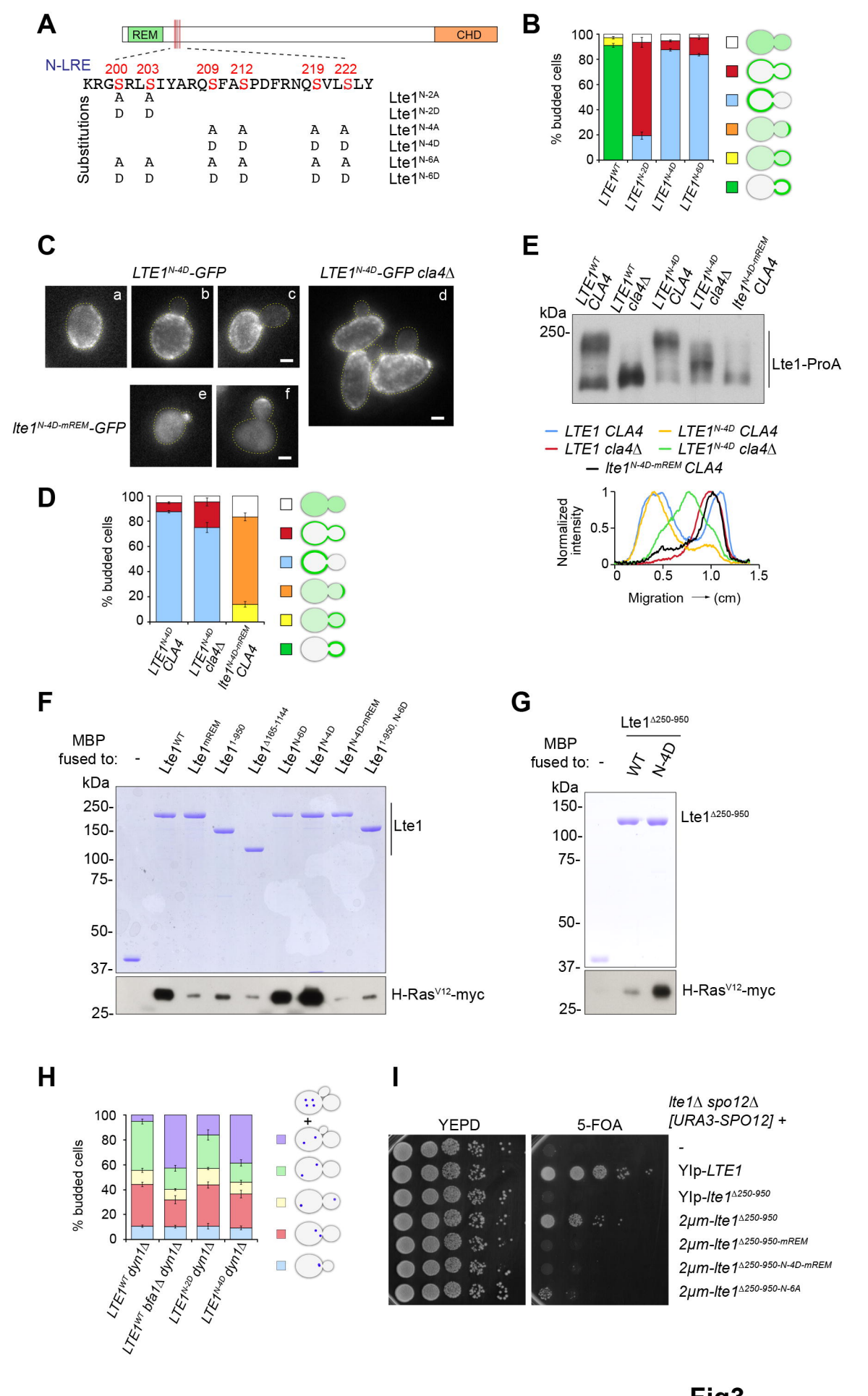
A
REM
CHD
N-LRE
200 203 209 212 219 222
KRGSRLSIYARQSFASPDFRNQSVLSLY
Substitutions
Lte1N-2A
Lte1N-2D
Lte1N-4A
Lte1N-4D
Lte1N-6A
Lte1N-6D
B
% budded cells
LTE1WT
LTE1N-2D
LTE1N-4D
LTE1N-6D
C
LTE1N-4D-GFP
LTE1N-4D-GFP cla4Δ
lte1N-4D-mREM-GFP
a
b
c
d
e
f
D
% budded cells
LTE1N-4D CLA4
LTE1N-4D cla4Δ
lte1N-4D-mREM CLA4
E
LTE1WT CLA4
LTE1WT cla4Δ
LTE1N-4D CLA4
LTE1N-4D cla4Δ
lte1N-4D-mREM CLA4
kDa
250-
Lte1-ProA
LTE1 CLA4
LTE1 cla4Δ
LTE1N-4D CLA4
LTE1N-4D cla4Δ
lte1N-4D-mREM CLA4
Normalized intensity
Migration → (cm)
F
MBP fused to:
-
Lte1WT
Lte1mREM
Lte11-950
Lte1Δ165-1144
Lte1N-6D
Lte1N-4D
Lte1N-4D-mREM
Lte11-950, N-6D
kDa
250-
150-
100-
75-
50-
37-
25-
Lte1
H-RasV12-myc
G
Lte1Δ250-950
MBP fused to:
-
WT
N-4D
kDa
150-
100-
75-
50-
37-
25-
Lte1Δ250-950
H-RasV12-myc
H
% budded cells
LTE1WT dyn1Δ
LTE1WT bfa1Δ dyn1Δ
LTE1N-2D dyn1Δ
LTE1N-4D dyn1Δ
+
I
YEPD
5-FOA
lte1Δ spo12Δ [URA3-SPO12] +
-
YIp-LTE1
YIp-lte1Δ250-950
2μm-lte1Δ250-950
2μm-lte1Δ250-950-mREM
2μm-lte1Δ250-950-N-4D-mREM
2μm-lte1Δ250-950-N-6A

Fig3

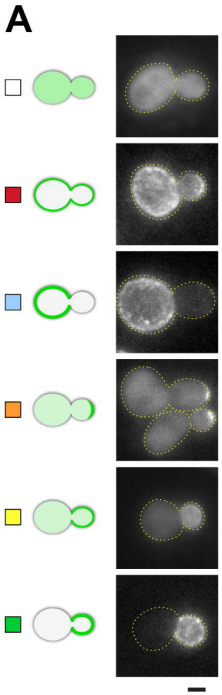

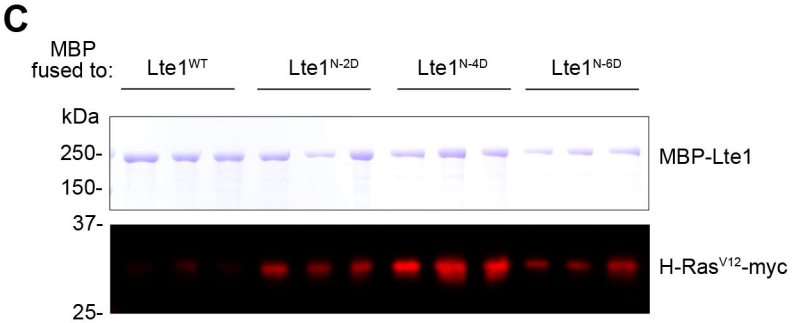

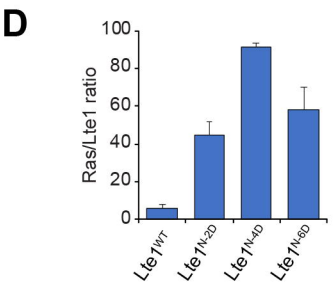

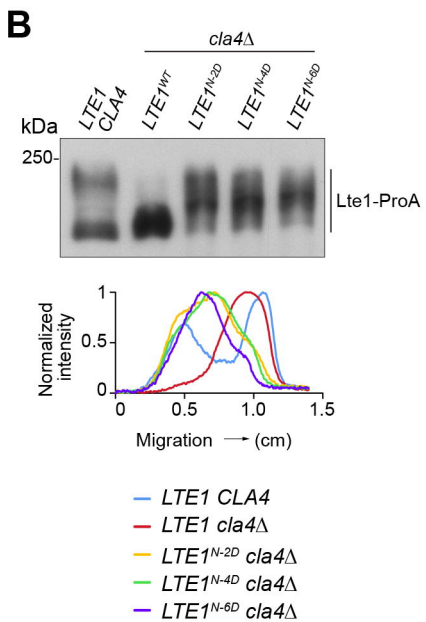

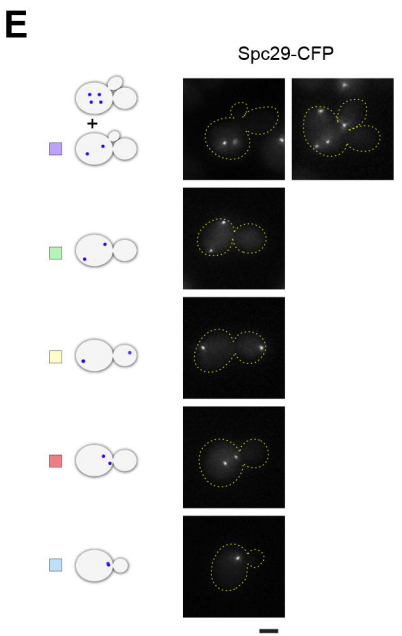

Suppl to Fig3

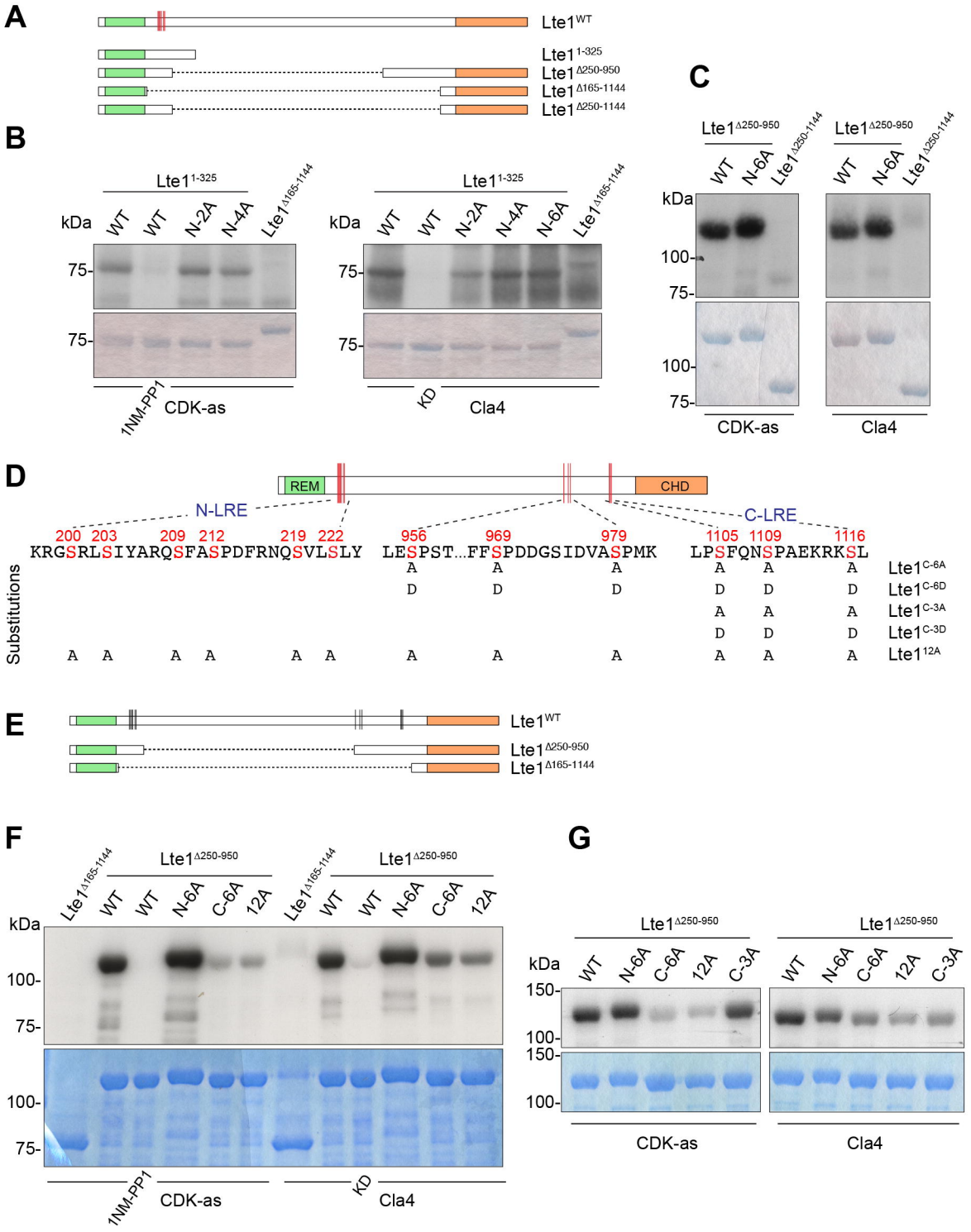
A
Lte1WT
Lte1 1-325
Lte1 Δ250-950
Lte1 Δ165-1144
Lte1 Δ250-1144
B
Lte1 1-325
kDa
WT
WT
N-2A
N-4A
Lte1 Δ165-1144
75-
75-
1NM-PP1
CDK-as
Lte1 1-325
kDa
WT
WT
N-2A
N-4A
N-6A
Lte1 Δ165-1144
75-
75-
KD
Cla4
C
Lte1 Δ250-950
WT
N-6A
Lte1 Δ250-1144
kDa
100-
75-
100-
75-
CDK-as
Lte1 Δ250-950
WT
N-6A
Lte1 Δ250-1144
Cla4
D
REM
CHD
N-LRE
C-LRE
200 203 209 212 219 222 956 969 979 1105 1109 1116
KRGSRLSIYARQSFASPDFRNQSVLSLY LESPST...FFSPDDGSIDVASPMK LPSFQNSPAEKRKSL
Substitutions
A A Lte1 C-6A
D D Lte1 C-6D
A A A Lte1 C-3A
D D D Lte1 C-3D
A A A A A A A A A A A A Lte1 12A
E
Lte1WT
Lte1 Δ250-950
Lte1 Δ165-1144
F
Lte1 Δ165-1144
Lte1 Δ250-950
WT
WT
N-6A
C-6A
12A
Lte1 Δ165-1144
Lte1 Δ250-950
WT
WT
N-6A
C-6A
12A
kDa
100-
75-
100-
75-
1NM-PP1
CDK-as
KD
Cla4
G
Lte1 Δ250-950
WT
N-6A
C-6A
12A
C-3A
kDa
150-
100-
150-
100-
CDK-as
Lte1 Δ250-950
WT
N-6A
C-6A
12A
C-3A
Cla4

Fig4

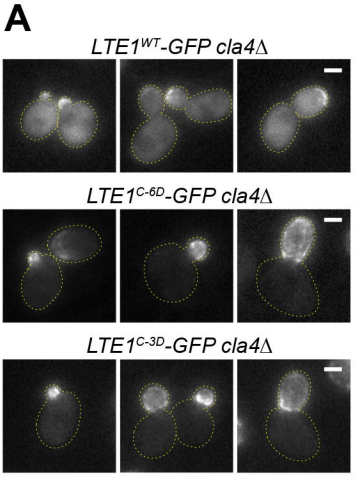
A
LTE1WT-GFP cla4Δ
LTE1C-6D-GFP cla4Δ
LTE1C-3D-GFP cla4Δ

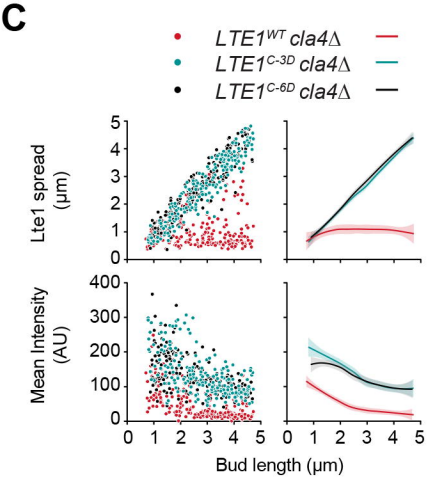
C
LTE1WT cla4Δ
LTE1C-3D cla4Δ
LTE1C-6D cla4Δ
Lte1 spread (µm)
Mean Intensity (AU)
Bud length (µm)

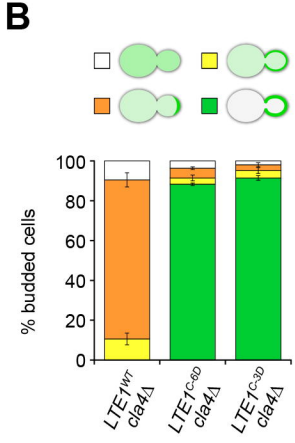
B
% budded cells
LTE1WT cla4Δ
LTE1C-6D cla4Δ
LTE1C-3D cla4Δ

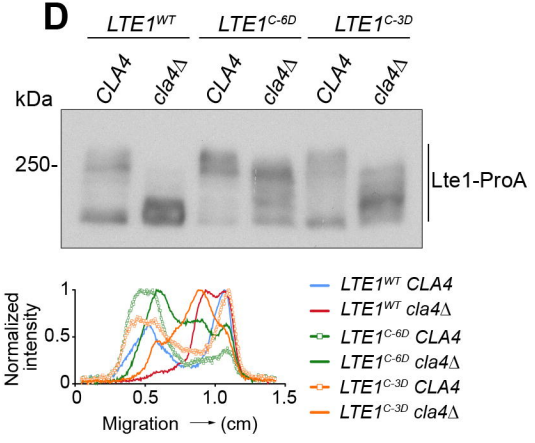
D
LTE1WT
LTE1C-6D
LTE1C-3D
CLA4
cla4Δ
kDa
250-
Lte1-ProA
Normalized intensity
Migration → (cm)
LTE1WT CLA4
LTE1WT cla4Δ
LTE1C-6D CLA4
LTE1C-6D cla4Δ
LTE1C-3D CLA4
LTE1C-3D cla4Δ

Fig5

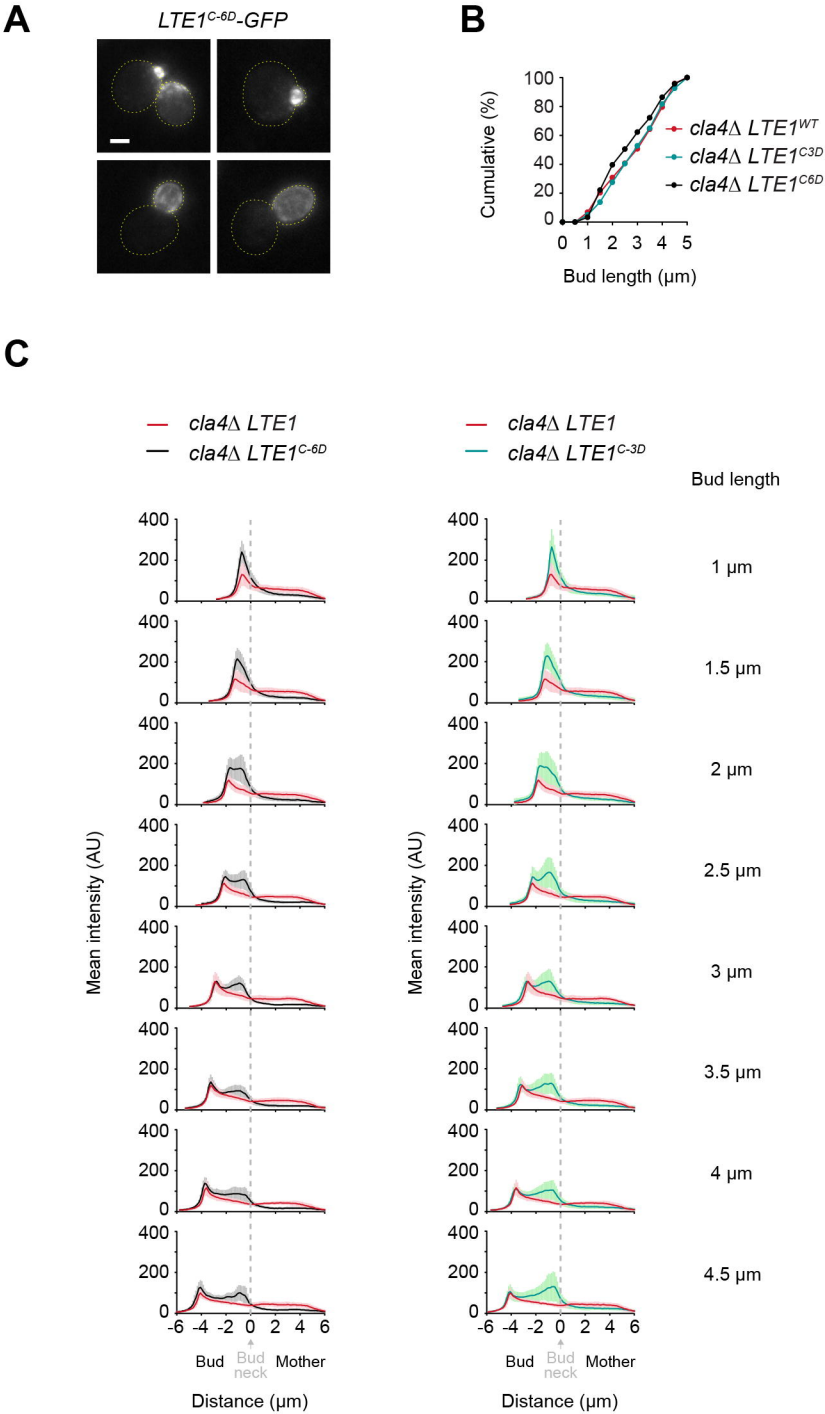

Suppl to Fig5

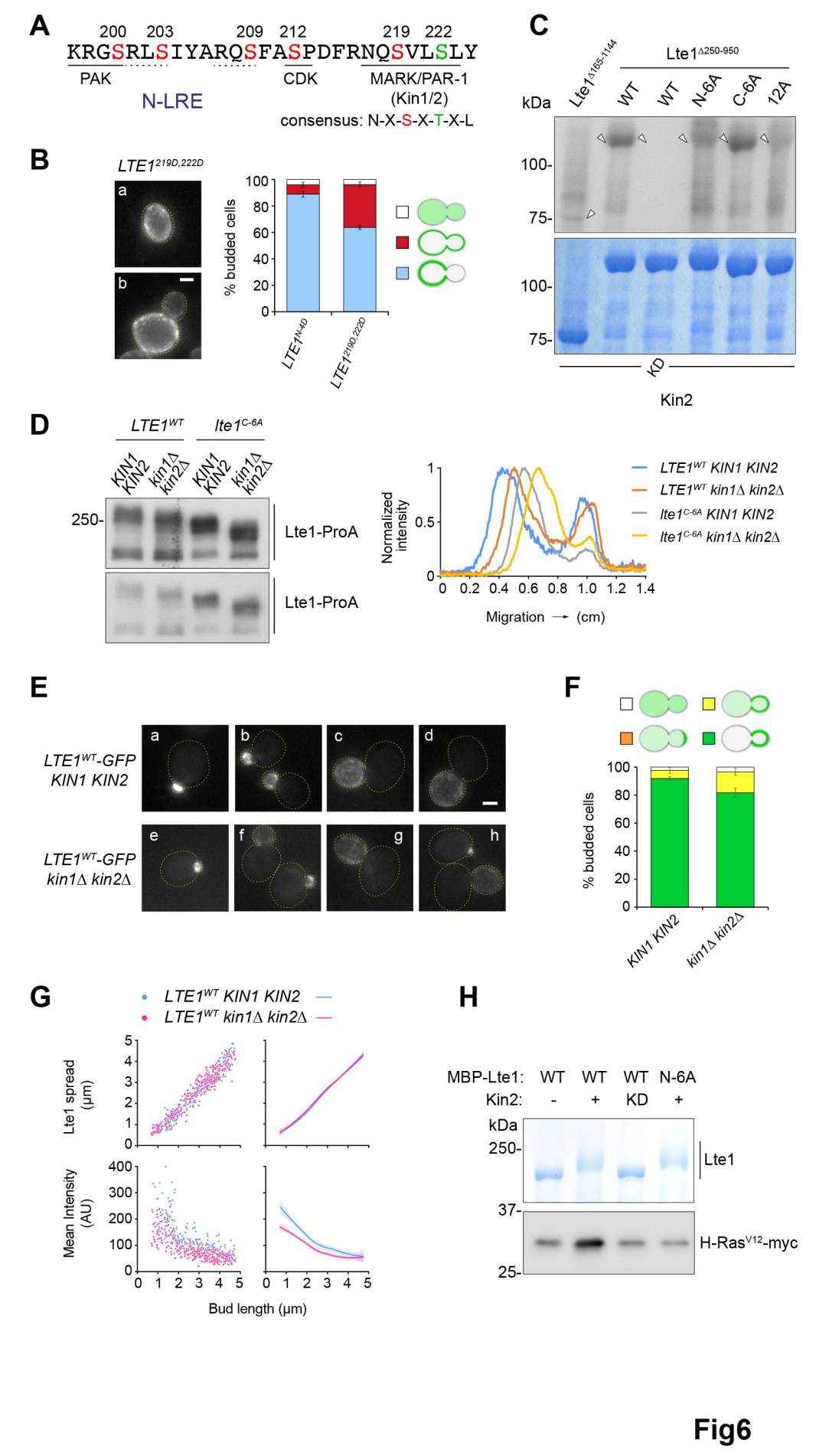
A
200 203 209 212 219 222
KRGSRLSIYARQSFASPDFRNQSVLSLY
PAK
CDK
MARK/PAR-1
(Kin1/2)
N-LRE
consensus: N-X-S-X-T-X-L
B
LTE1219D,222D
a
b
% budded cells
LTE1N-4D
LTE1219D,222D
C
Lte1Δ250-950
Lte1Δ165-1144
WT
WT
N-6A
C-6A
12A
kDa
100-
75-
KD
Kin2
D
LTE1WT
lte1C-6A
KIN1 KIN2
kin1Δ kin2Δ
250-
Lte1-ProA
Normalized intensity
Migration → (cm)
LTE1WT KIN1 KIN2
LTE1WT kin1Δ kin2Δ
lte1C-6A KIN1 KIN2
lte1C-6A kin1Δ kin2Δ
E
LTE1WT-GFP
KIN1 KIN2
LTE1WT-GFP
kin1Δ kin2Δ
F
% budded cells
KIN1 KIN2
kin1Δ kin2Δ
G
LTE1WT KIN1 KIN2
LTE1WT kin1Δ kin2Δ
Lte1 spread (µm)
Mean Intensity (AU)
Bud length (µm)
H
MBP-Lte1: WT WT WT N-6A
Kin2: - + KD +
kDa
250-
37-
25-
Lte1
H-RasV12-myc

Fig6

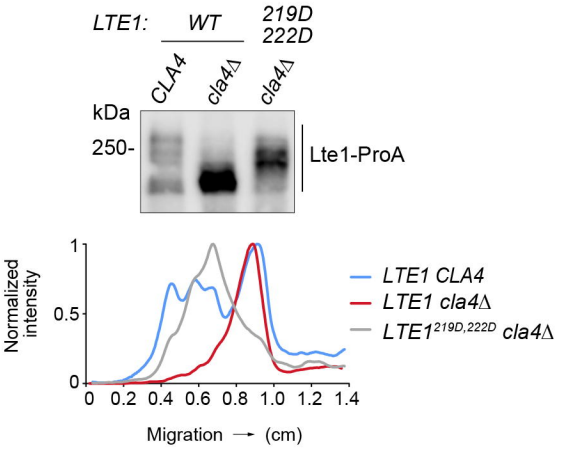

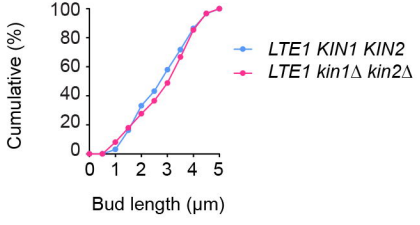

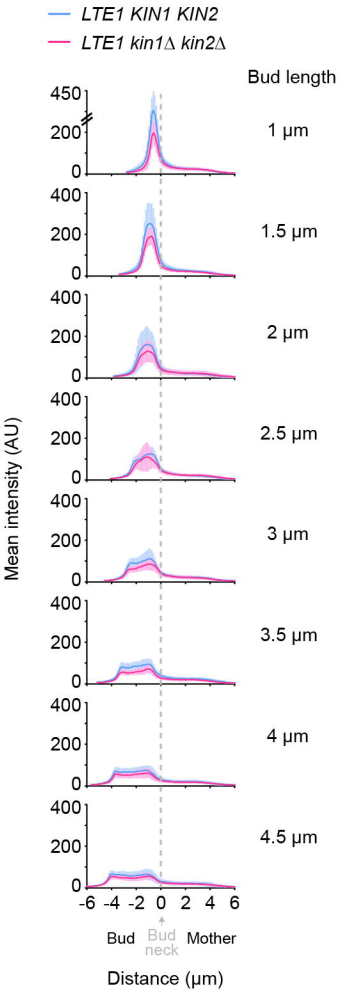

Suppl to Fig6

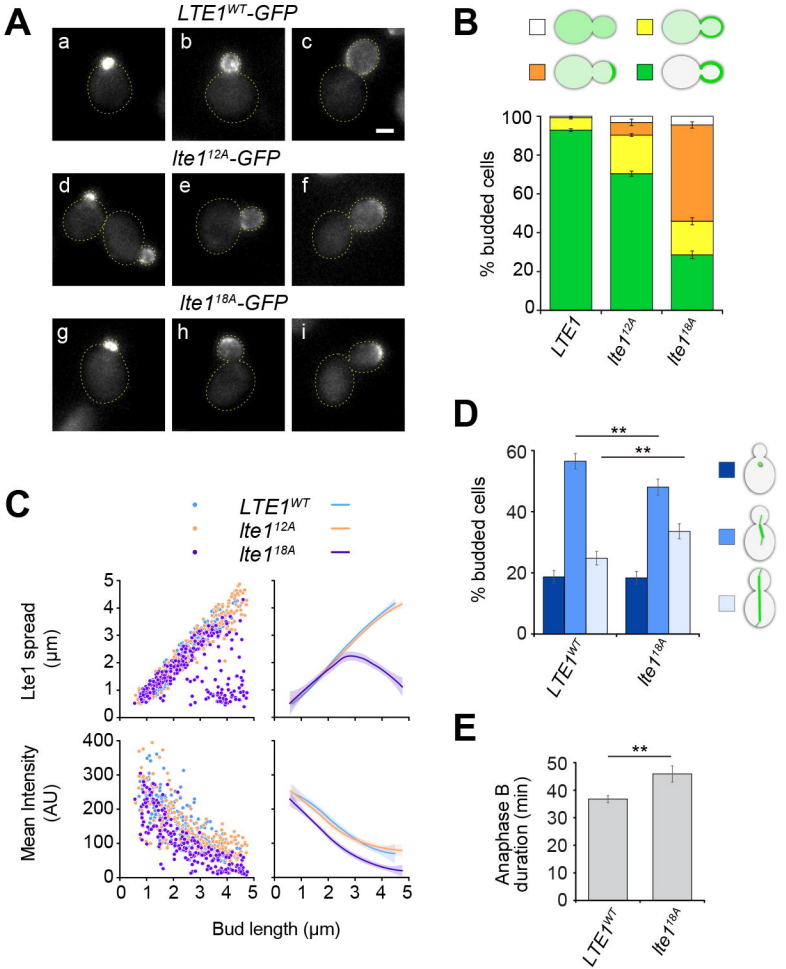
A
LTE1WT-GFP
a
b
c
lte112A-GFP
d
e
f
lte118A-GFP
g
h
i
B
% budded cells
100
80
60
40
20
0
LTE1
lte112A
lte118A
C
LTE1WT
lte112A
lte118A
Lte1 spread (µm)
Mean Intensity (AU)
Bud length (µm)
D
% budded cells
**
**
LTE1WT
lte118A
E
Anaphase B duration (min)
**
LTE1WT
lte118A

Fig7

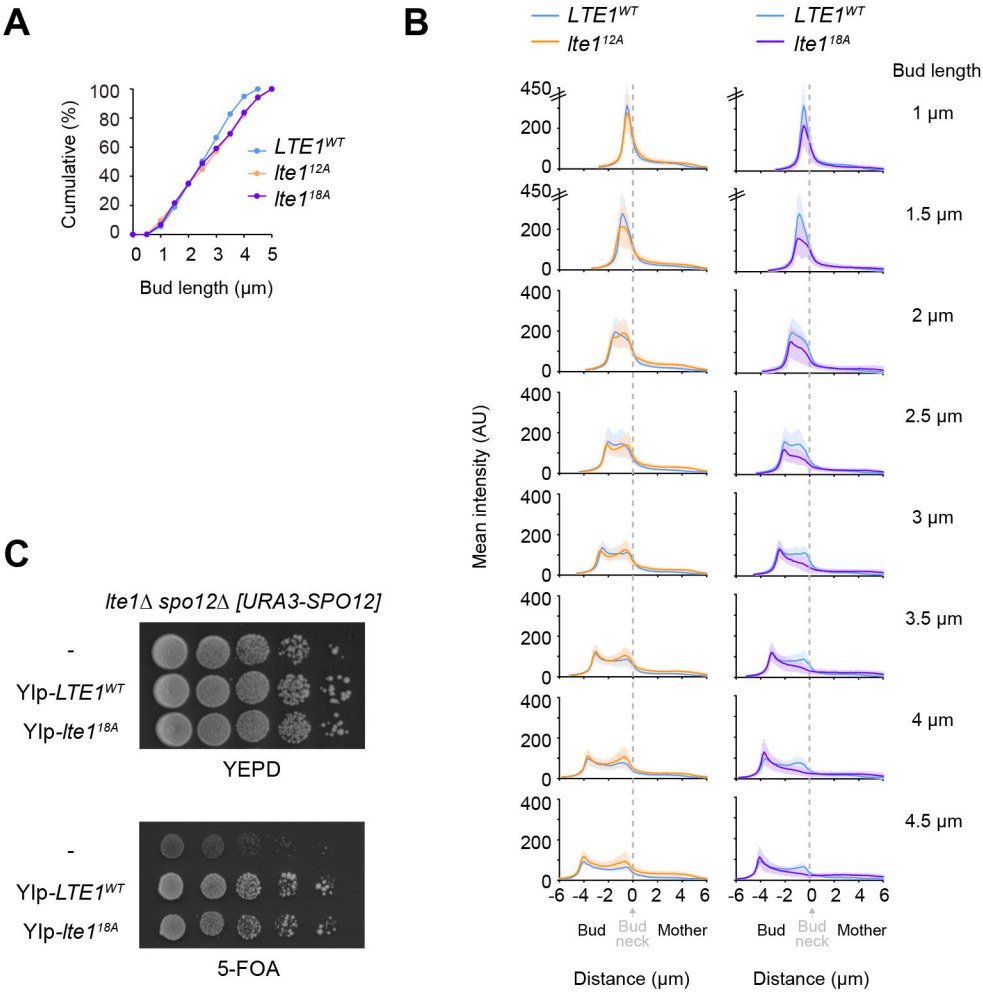

Suppl to Fig 7

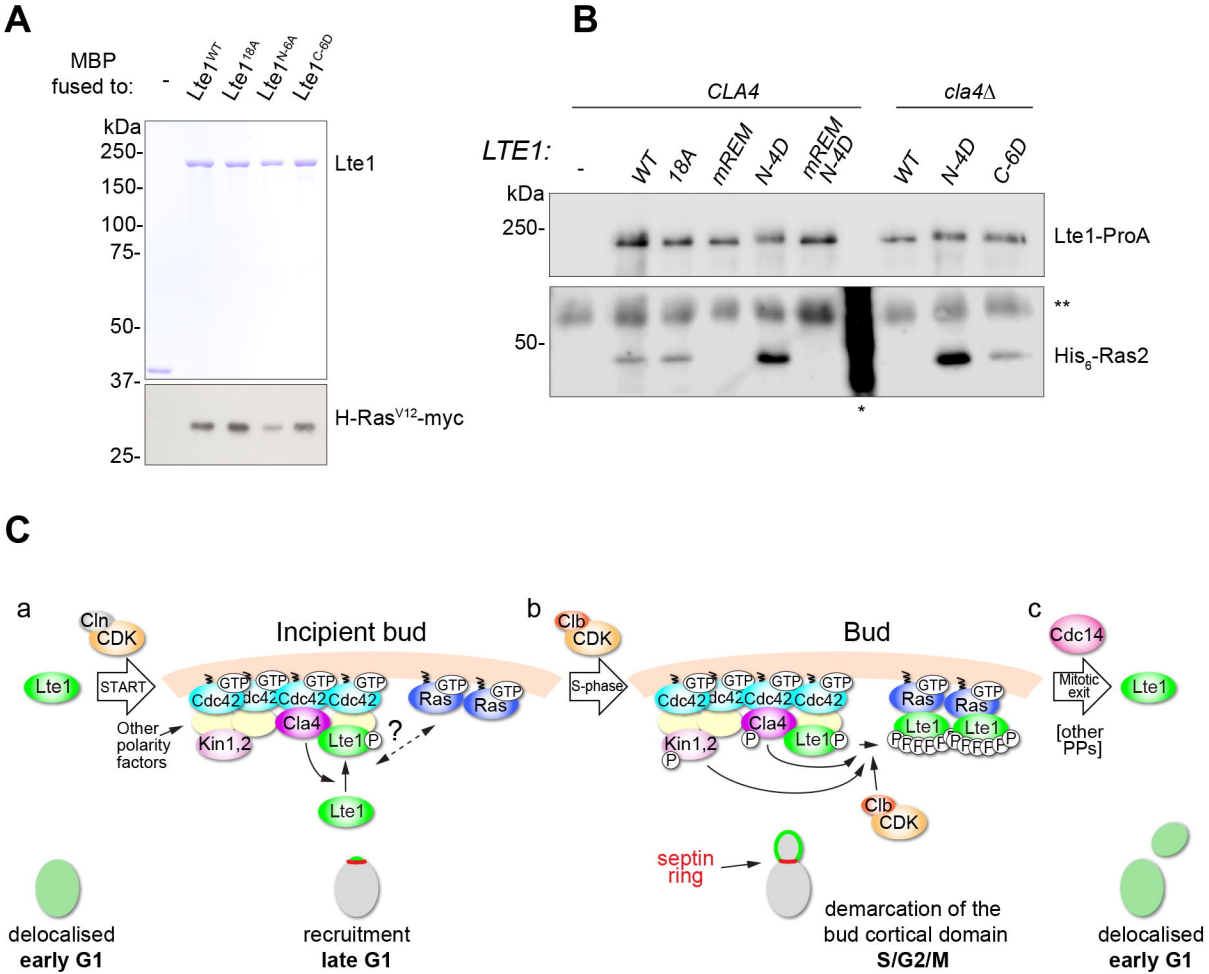
A
MBP fused to:
-
Lte1WT
Lte1 18A
Lte1N-6A
Lte1C-6D
kDa
250-
150-
100-
75-
50-
37-
25-
Lte1
H-RasV12-myc
B
CLA4
cla4Δ
LTE1:
-
WT
18A
mREM
N-4D
mREM N-4D
WT
N-4D
C-6D
kDa
250-
50-
Lte1-ProA
**
His6-Ras2
*
C
a
Cln
CDK
Lte1
START
Other polarity factors
Incipient bud
GTP
Cdc42
Ras
Cla4
Kin1,2
Lte1
P
?
Lte1
delocalised
early G1
recruitment
late G1
b
Clb
CDK
S-phase
Bud
Cdc42
Ras
Cla4
Kin1,2
Lte1
P
Clb
CDK
septin ring
demarcation of the bud cortical domain
S/G2/M
c
Cdc14
Mitotic exit
[other PPs]
Lte1
delocalised
early G1

Fig8